Stem Cell Reports
Article

ISSCR

OPEN ACCESS

# Stabilization of cell-cell adhesions prevents symmetry breaking and locks in pluripotency in 3D gastruloids

Federica Cermola,[1,4] Filomena Amoroso,[1,2,4] Federica Saracino,[1] Eduardo Ibello,[1,2] Dario De Cesare,[1] Annalisa Fico,[1] Gilda Cobellis,[2] Enrica Scalera,[3] Costanza Casiraghi,[3] Cristina D'Aniello,[1] Eduardo Jorge Patriarca,[1,*] and Gabriella Minchiotti[1,*]

[1]Stem Cell Fate Laboratory, Institute of Genetics and Biophysics "A. Buzzati Traverso", CNR, Naples, Italy
[2]Department of Precision Medicine, University of Campania Luigi Vanvitelli, Naples, Italy
[3]Pharmacology and Toxicology Department, Corporate Pre-clinical R&D, Chiesi, Parma, Italy
[4]These authors contributed equally
*Correspondence: eduardo.patriarca@igb.cnr.it (E.J.P.), gabriella.minchiotti@igb.cnr.it (G.M.)
https://doi.org/10.1016/j.stemcr.2022.09.013

## SUMMARY

3D embryonic stem cell (ESC) aggregates self-organize into embryo-like structures named gastruloids that recapitulate the axial organization of post-implantation embryos. Crucial in this process is the symmetry-breaking event that leads to the emergence of asymmetry and spatially ordered structures from homogeneous cell aggregates. Here, we show that budesonide, a glucocorticoid drug widely used to treat asthma, prevents ESC aggregates to break symmetry. Mechanistically, the effect of budesonide is glucocorticoid receptor independent. RNA sequencing and lineage fate analysis reveal that budesonide counteracts exit from pluripotency and modifies the expression of a large set of genes associated with cell migration, A-P axis formation, and WNT signaling. This correlates with reduced phenotypic and molecular cell heterogeneity, persistence of E-CADHERIN at the cell-cell interface, and cell aggregate compaction. Our findings reveal that cell-cell adhesion properties control symmetry breaking and cell fate transition in 3D gastruloids and suggest a potential adverse effect of budesonide on embryo development.

## INTRODUCTION

Pluripotent embryonic stem cells (ESCs) have a propensity to self-organize into tightly packed cell aggregates sustained by anchoring cell-cell junctions (Pieters and van Roy, 2014). Naive pluripotent ESCs form domed-shaped cell colonies and spherical cell aggregates under 2D and 3D conditions, respectively, whereas exit from naive pluripotency is associated with weakening of the cell-cell adhesive interactions and acquisition of cell motility. Whether exit from naive pluripotency and reprogramming of the cell-cell interactions are mutually dependent is still debated.

Exit from naive pluripotency and acquisition of cell motility is a key feature of embryonic stem cell-to-mesenchymal-like transition (esMT), which is induced by proline supplementation in 2D culture conditions (Comes et al., 2013; Patriarca et al., 2021). Under a high-proline/low-ascorbic acid (vitamin C) regimen, serum/LIF ESCs exit naive pluripotency and grow as irregular flat-shaped colonies surrounded by a crown of free migrating cells (Comes et al., 2013; D'Aniello et al., 2017). These early primitive ectoderm-like (Washington et al., 2010) or proline-induced cells (PiCs) (Casalino et al., 2011) show transcriptome, epigenetic, and metabolic profile resembling that of early-primed pluripotent state (Comes et al., 2013; D'Aniello et al., 2015; D'Aniello et al., 2017), suggesting that they are part of the formative pluripotency (Morgani et al., 2017; Pera and Rossant, 2021; Smith, 2017).

In 3D culture, floating aggregates of ESCs self-organize into embryo-like structures named gastruloids, which display key features of mammalian development after implantation (Turner et al., 2017; van den Brink et al., 2020; van den Brink et al., 2014). This self-organization process is associated with induction of collective cell migration (Hashmi et al., 2021). Formation of appropriate cell aggregates is a critical event for the generation of properly elongated gastruloids (Cermola et al., 2021; Turner et al., 2017), yet the mechanisms that trigger symmetry breaking and induce cell fate specification in spheroidal aggregates of ESCs are still far from being fully elucidated.

Here, we adopt a chemical genetic approach to perturb ESC self-organization processes and investigate the cellular mechanisms underlying symmetry breaking. Different from the genetic approaches, small molecules are easy to apply to cells and may often work reversibly (Kawasumi and Nghiem, 2007), which is relevant to investigate dynamic cellular processes and morphogenesis. Our findings provide unprecedented evidence that the glucocorticoid budesonide, the most commonly used drug to treat asthma, interferes with the self-organizing ability of cell populations promoting cell-cell adhesion and preventing exit from pluripotency through a glucocorticoid receptor (GR)-independent mechanism.

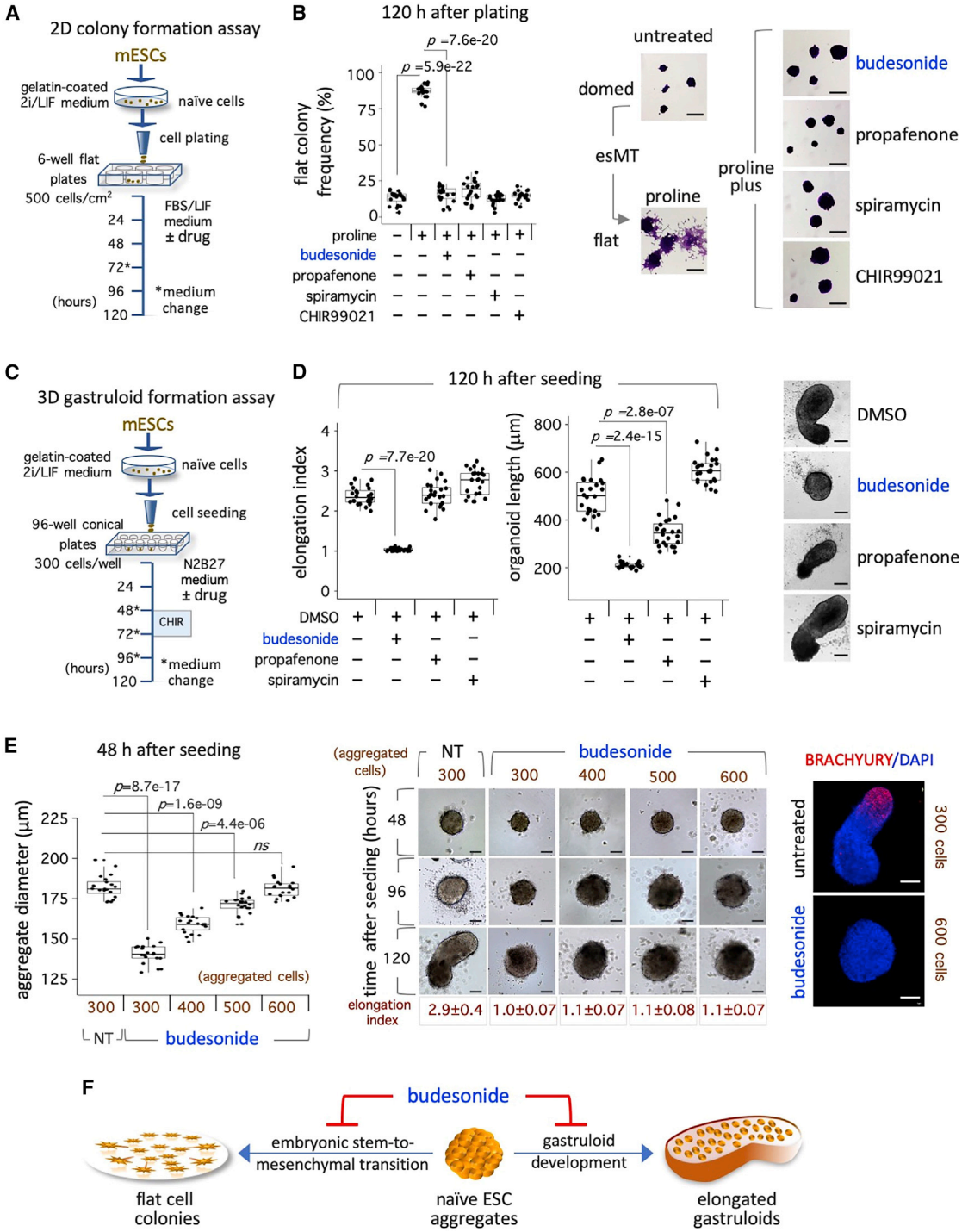


**Figure 1. Effect of esMT inhibitors on colony morphology and gastruloid formation**

(A) Schematic representation of the experimental design. 2i/LIF ESCs (E14) were plated on gelatin-coated plates in FBS/LIF ± proline (500 μM) ± drug (10 μM). Cell colonies were stained with crystal violet and imaged.

(B) Boxplot diagram of the fraction (%) of irregular/flat colonies (left) and representative bright-field images (right) of the cell colonies (n = 4; 20 fields/condition). Scale bar, 200 μm.

(C) Schematic representation of the experimental design. 2i/LIF ESCs were plated on 96-well ultra-low conical plates in N2B27 ± drug (10 μM).

*(legend continued on next page)*

## RESULTS

### The glucocorticoid budesonide prevents gastruloid elongation

To probe the plasticity of the symmetry breaking process, we sought to assess the effect on gastruloid formation of three FDA-approved drugs, budesonide (steroid), propafenone (phenylpropanoid), and spiramycin (macrolide), recently identified as inhibitors of esMT in the feeder-dependent TBV2 ESCs (D'Aniello et al., 2019).

We first verified that the selected drugs were similarly effective on the feeder-independent E14 ESC line. ESCs were thus plated at low density in FBS/LIF supplemented with proline to induce esMT, either alone or in the presence of budesonide, propafenone, and spiramycin, or the GSK-3 inhibitor CHIR99021 (CHIR) as a positive control (D'Aniello et al., 2019), and the distribution of flat versus domed colonies was analyzed as a readout of esMT (Figures 1A and 1B). Addition of either budesonide, propafenone, spiramycin, or CHIR reduced the fraction of irregular/flat-shaped cell colonies in proline-treated cell population (FBS/LIF + proline ~90%) to control levels (FBS/LIF ~15%) (Figure 1B). As expected, the ESC colonies showed a highly compacted morphology (Figure 1B), thus ruling out the possibility of an ESC line-specific effect of the esMT inhibitors (esMTi).

We thus evaluated the effect of esMTi on gastruloid formation (Cermola et al., 2021, 2022) (Figure 1C). Budesonide, propafenone, and spiramycin (10 μM) were added at T = 0 and refreshed every day from day 2 onward. At 120 h after seeding, gastruloids were imaged, the width and length (LN) were measured, and the elongation index (EI = length/width) was calculated. While control aggregates developed into highly polarized gastruloids (EI = 2.3 ± 0.2), budesonide-treated aggregates maintained a round-shaped spherical morphology (EI = 1.03 ± 0.04) and failed to elongate (Figures 1D and S1A). Conversely, spiramycin- and propafenone-treated aggregates developed into elongated gastruloids (EI = 2.8 ± 0.3 and 2.4 ± 0.3, respectively). However, although both spiramycin- and propafenone-treated gastruloids showed a correct EI (Figures 1D and S1A), propafenone-treated gastruloids appeared shorter (LN = 345 ± 58 μm) compared with both spiramycin-treated and untreated gastruloids (LN = 606 ± 51 m and 501 ± 74 μm, respectively) (Figures 1D and S1A).

The diameter of ESC aggregates is a critical parameter for successful gastruloid development (Turner et al., 2017). Therefore, we increased the number of aggregated cells (300–600) and evaluated the effect of budesonide on gastruloid development. The diameter of budesonide-treated cell aggregates (48 h) progressively increased with the number of seeded cells (Figure 1E), reaching a diameter comparable with that of control at 600 cells (control 300 cells 182.25 ± 7.15 μm versus budesonide 600 cells 181 ± 5.5 μm). However, budesonide-treated aggregates did not elongate and maintained a round-shaped morphology at 120 h (Figure 1E), even when reaching the size of control aggregates at 48 h. Furthermore, unlike control gastruloids, budesonide-treated aggregates did not express BRACHYURY, independently from the numbers of seeded cells (Figures 1E and S1B).

These data highlight a distinctive/peculiar ability of budesonide to prevent changes in the shape of both 2D cell colonies (esMT) and 3D aggregates (gastruloid elongation) (Figure 1F).

### Budesonide inhibits esMT and gastruloid development in the same range of concentrations without affecting cell proliferation

Gastruloid development and proline-induced esMT both depend on the acquisition of cell locomotion capability. To investigate whether budesonide may target different molecules/pathways in 2D versus 3D culture conditions, we compared the dose-dependent effect of budesonide on both processes (Figure 2). As a readout of esMT we analyzed the distribution of irregular flat- versus domed-shaped colonies in ESCs treated with proline ± budesonide. As expected, the fraction of flat-shaped irregular colonies increased upon proline supplementation compared with control (87% ± 7% versus 11% ± 4%), while it progressively decreased as the concentration of budesonide increased from 1.25 to 10 μM, and reached a value comparable with that of control (Figure 2A).

We then analyzed the dose-dependent effect of budesonide on gastruloid development, and calculated the elongation index as a readout of the process. Control DMSO-treated cell aggregates developed into highly polarized gastruloids at 120 h (EI = 2.8 ± 0.3) (Figures 2B and S1C). In a range of concentration from 1.25 to 2.5 μM, budesonide did not affect gastruloids elongation. However, at

(D) Boxplot diagrams of gastruloid elongation index (left) and length distribution (middle), and representative bright-field images (right) of gastruloids treated with DMSO (control) or the indicated drugs (n = 3; 24 gastruloids/condition). Scale bar, 100 μm.
(E) Boxplot diagram of the diameter values of ESC ± budesonide-derived aggregates (left; 48 h, n = 3; 20 aggregates/condition); time-course representative bright-field images of ESCs ± budesonide-derived gastruloids and elongation index values at 120 h (middle; n = 3; 30 aggregates/condition). Scale bar, 100 μm. Representative confocal images of BRACHYURY at 120 h (right). Nuclei were counterstained with DAPI (blue). Scale bar, 100 μm. NT, not treated.
(F) Schematic representation of the effect of budesonide on 2D esMT and 3D gastruloid elongation. See also Figure S1.

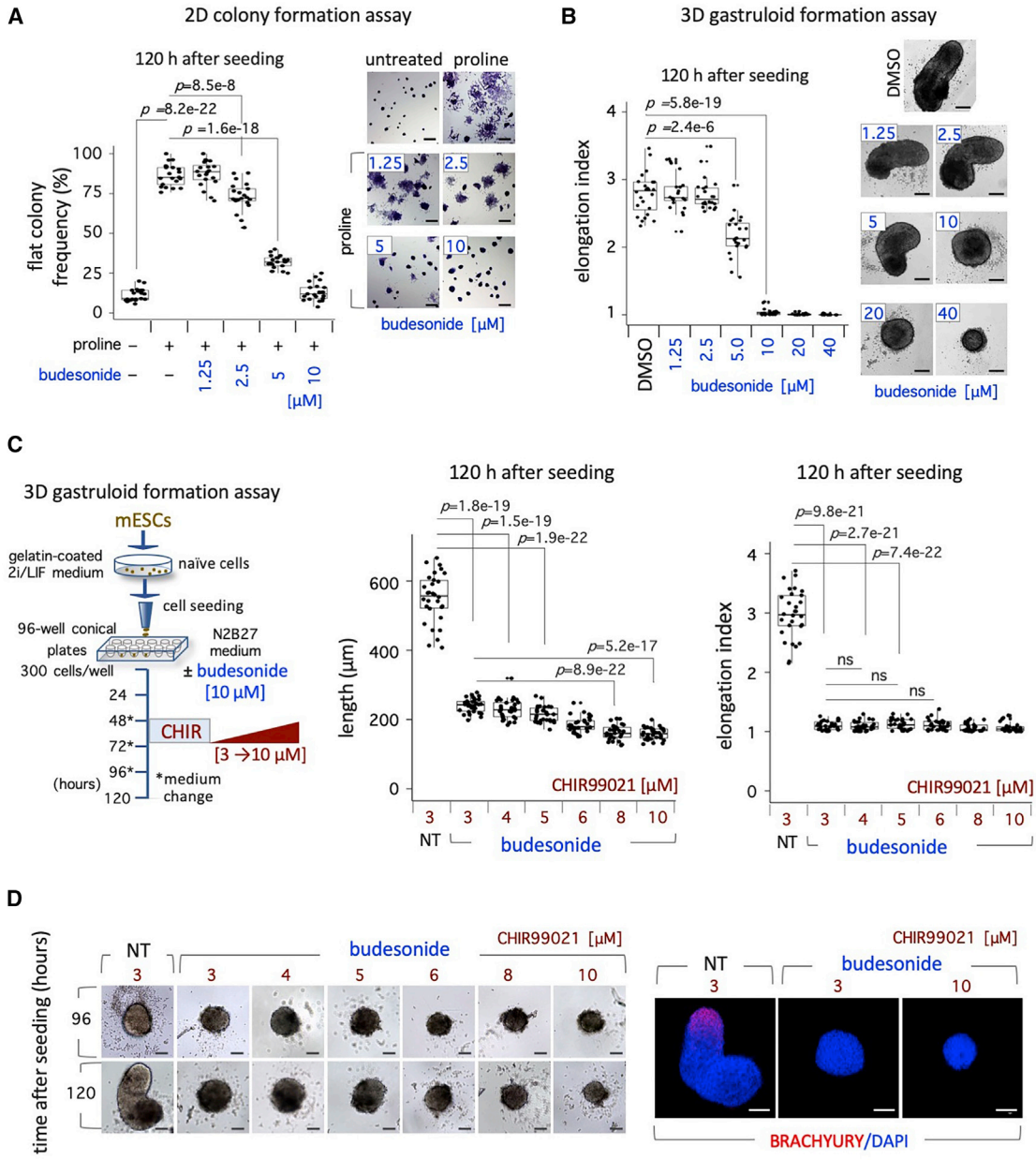


**Figure 2. Dose-dependent effect of budesonide on colony morphology and gastruloid elongation**

(A) Boxplot diagram of the fraction (%) of irregular/flat colonies (left) in FBS/LIF ± proline (500 μM) ± budesonide (1.25–10 μM), and representative bright-field images (right) of the colonies (n = 3; 21 fields/condition). Scale bar, 200 μm.

(B) Boxplot diagram of the elongation index (left), and representative bright-field images (right) of control (DMSO) or budesonide (1.25–40 μM)-treated gastruloids (n = 3; 24 gastruloids/condition). Scale bar, 50 μm.

(C) Dose-dependent effect of CHIR99021 on budesonide-treated gastruloids. 2i/LIF ESCs were seeded in N2B27 ± budesonide (10 μM), CHIR99021 (3–10 μM) was added at 48–72 h (left). Boxplot diagram of gastruloid length distribution (middle) and elongation index (right) at 120 h. NT, not treated.

(D) Representative bright-field images of gastruloids ± budesonide (10 μM) + CHIR99021 (3–10 μM) (left), and confocal images of BRACHYURY (red) in gastruloids (120 h) ± budesonide (10 μM) + CHIR99021 (3 and 10 μM) (right). Nuclei were counterstained with DAPI (blue). Scale bar, 100 μm. See also Figures S1 and S2.

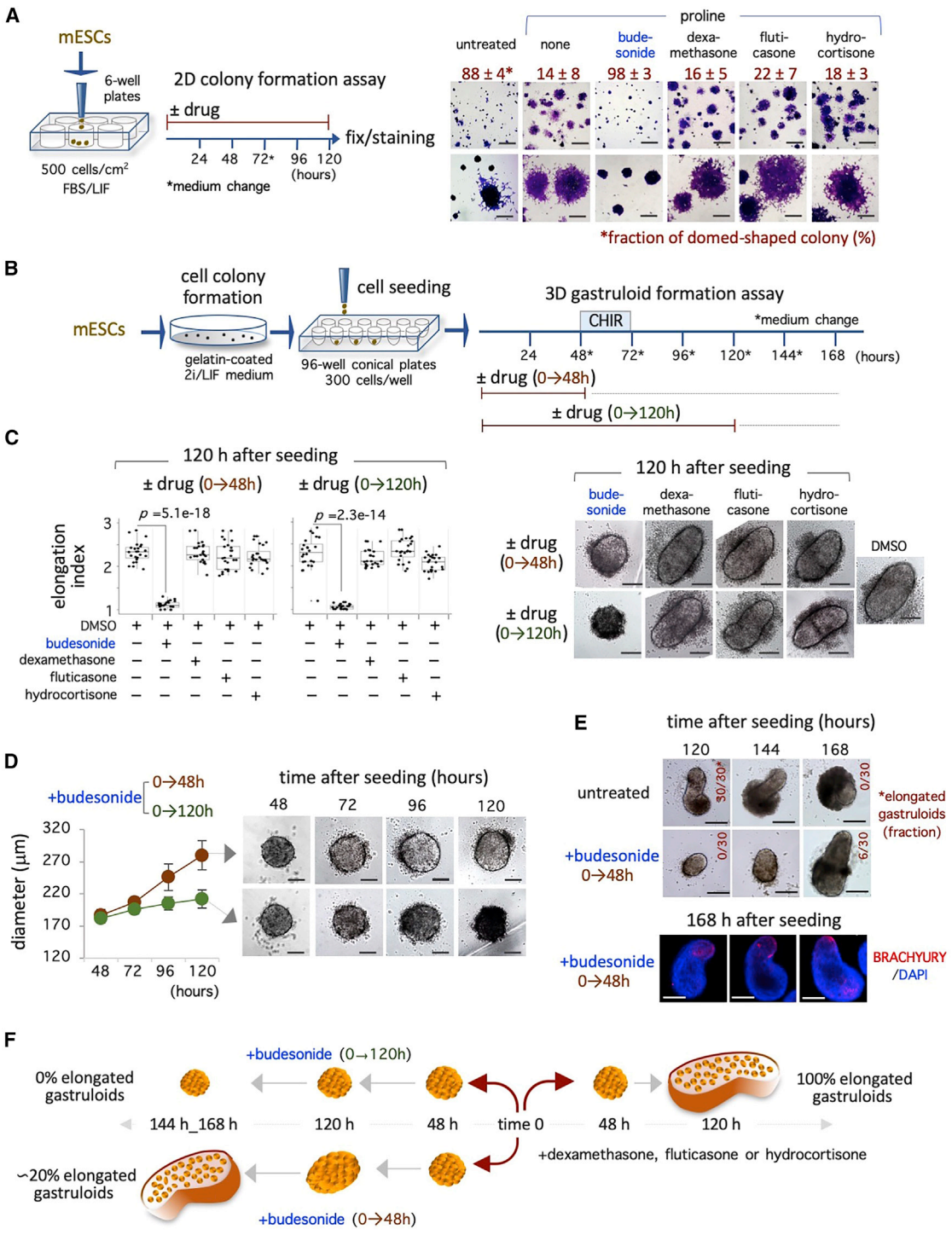


**Figure 3. Effect of the typical glucocorticoids on colony morphology and gastruloid elongation**

(A) Schematic representation of the colony formation assay (left) and representative images (right) at low (top) and high (bottom) magnification of FBS/LIF ESCs ± proline (500 µM) ± glucocorticoids (10 µM). The fraction of domed-shaped cell colonies is indicated (n = 3; >300 colonies/condition). Scale bar, 200 µm.

(B) Schematic representation of the experimental design. Naive ESCs were plated in N2B27 in ultra-low 96-well plates ± the indicated drugs (10 µM) for 0–48 h (brown orange) or 0–120 h (green).

*(legend continued on next page)*

5 μM a significant reduction of the gastruloid elongation was observed (EI = 2.1 ± 0.3), while at higher concentrations, ranging from 10 to 40 μM, budesonide-treated gastruloids showed a round-shaped spherical morphology (EI = 1.0 ± 0.1) and failed to elongate (Figures 2B and S1C).

To rule out the possibility that budesonide might counteract the inductive effect of CHIR at the concentration used (3 μM), we asked whether higher concentrations of CHIR could overcome budesonide-dependent inhibition of gastruloid formation. To this end, we assessed the dose-dependent effect of CHIR (3–10 μM) on budesonide-treated gastruloids (Figure 2C). At all tested concentrations of CHIR, budesonide-treated aggregates failed to elongate and did not express BRACHYURY at 120 h (Figures 2C and 2D), indicating that higher doses of CHIR were not able to counteract the inhibitory effect of budesonide on gastruloid elongation. Of note, highest concentrations of CHIR (8–10 μM) resulted in smaller and apparently unhealthy aggregates (Figures 2D and S1D).

To investigate whether the budesonide-dependent inhibition of esMT and gastruloid formation might be due to an antiproliferative effect of the drug on ESCs, we first analyzed the dose-dependent effect of budesonide on the incorporation of 5-ethynyl-2′-deoxyuridine (EdU). EdU incorporation was not affected in FBS/LIF ESCs treated with budesonide up to 10 μM, whereas it decreased to about 70% at 20 μM (Figure S2A) and was almost abolished at 40 μM (Figure S2A). In line with these findings, FACS analysis of Annexin V/propidium iodide staining showed that 5 and 10 μM of budesonide did not induce apoptosis, while a significant increase of apoptotic cells was observed at 40 μM of budesonide (Figure S2A). Thus, budesonide concentrations (10 μM) that inhibit both esMT and gastruloid formation neither affect proliferation nor induce apoptosis in ESCs.

Furthermore, we performed immunofluorescence analysis of the proliferation marker Ki67 on 3D gastruloids, and showed that it was expressed both in control and budesonide-treated gastruloids at 120 h (Figure S2B), suggesting that budesonide concentrations that block esMT and gastruloid formation did not affect ESC proliferation.

Together these data reveal that budesonide inhibits esMT and gastruloid elongation at a similar micromolar concentration range, and rule out the possibility that inhibition of gastruloid development may be due to a counteracting effect of budesonide on CHIR activity. In line with this idea, while budesonide inhibits both esMT and gastruloid development, CHIR exerts opposite effects on the two processes, i.e., inhibitory (Figure 1A) (D'Aniello et al., 2019) and inducing, respectively.

## The classical glucocorticoids do not affect esMT and gastruloid development

Budesonide belongs to a family of anti-inflammatory steroids, and binds to different steroid hormones receptors, including glucocorticoid, mineralocorticoid, and progesterone receptors within a nanomolar (nM) range (BindingDB: BDBM50354850). These doses are much lower than the micromolar (μM) concentrations at which budesonide inhibits esMT and gastruloid development. To investigate this further, we compared the effect of the classical glucocorticoids dexamethasone, fluticasone, and hydrocortisone with that of budesonide in both 2D (esMT) and 3D (gastruloids) assays.

We first evaluated the effect of glucocorticoids on esMT by analyzing the distribution of domed- versus irregular flat-shaped colonies in ESCs treated with proline ± glucocorticoids (Figure 3A). As expected, while proline reduced the fraction of domed-shaped colonies to ~15% compared with control (untreated; ~90%), budesonide (10 μM) increased this fraction up to control level. Conversely, neither dexamethasone, fluticasone, nor hydrocortisone used at the same concentrations (10 μM) were able to rescue the fraction of the domed-shaped colonies (Figure 3A), supporting the idea of a specific inhibitory effect of budesonide on esMT. We then evaluated the dose-dependent effect of the different drugs using a range of concentrations from 10 to 80 μM. Dexamethasone and hydrocortisone showed similar results at all the concentrations tested, while budesonide was toxic at 80 μM (Figures S3B and S3C). Fluticasone showed a partial inhibitory effect at 20 μM (~50% domed colonies), and was toxic at the highest concentrations (40 and 80 μM) (Figures S3B and S3C).

We then went on to investigate the effect of both short- and long-term treatment of glucocorticoids on 3D gastruloid development. Glucocorticoids were individually added either transiently (0–48 h) or throughout (0–120 h) the GFA, and the aggregates were imaged and measured at 48 and 120 h after seeding (Figure 3B). At 48 h, both

(C) Boxplot diagrams of the elongation index (left) and representative bright-field images (right) of gastruloids (120 h) at the indicated treatment (n = 3; 24 gastruloids/condition). Scale bar, 100 μm.

(D) Time-course analysis of diameter distribution (left) and representative bright-field images (right) of budesonide-treated aggregates. Scale bar, 100 μm.

(E) Representative bright-field images of gastruloids ± budesonide (0–48 h, 10 μM) at 120, 144, and 168 h after seeding. Scale bar, 200 μm (top). The fraction (%) of elongated gastruloids is indicated in red. Representative confocal images of BRACHYURY in gastruloids + budesonide (bottom). Nuclei were counterstained with DAPI. Scale bar, 100 μm.

(F) Schematic representation of the effect of glucocorticoids on gastruloid development. See also Figures S3 and S4.

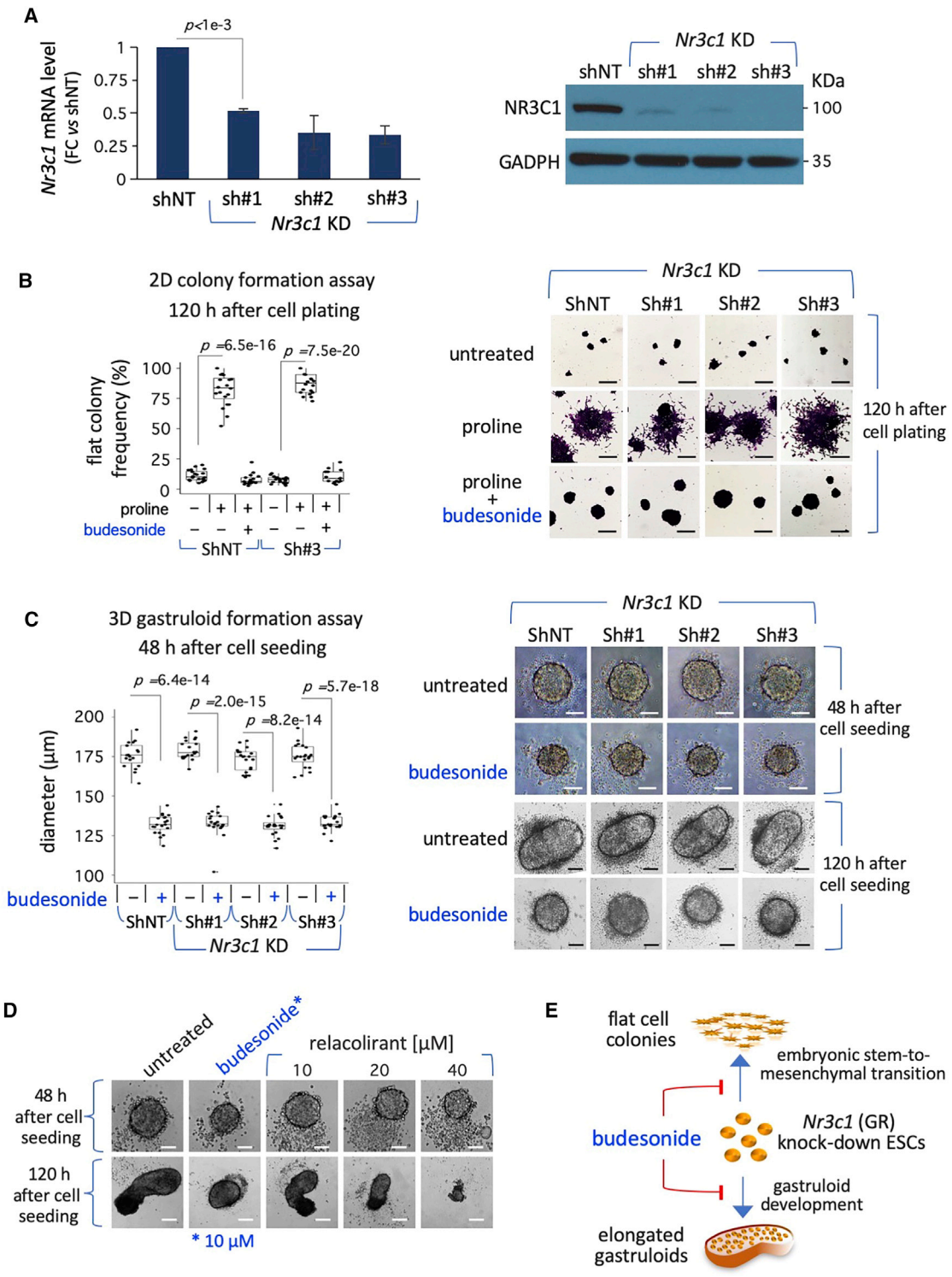


**Figure 4. Effect of budesonide on Nr3c1/GR knockdown ESCs**

(A) qPCR analysis of Nr3c1 in control (shNT) and *Nr3c1*KD (sh#1,2,3) ESCs (left). Data are fold change versus control, normalized to Gapdh and are mean ± SD (n = 3; p < 0.001). Western blot analysis of NR3C1 protein in control (shNT) and *Nr3c1*KD ESCs (right); anti-GAPDH antibodies were used as loading control.

*(legend continued on next page)*

the shape and the size of the cellular aggregates treated with either dexamethasone, fluticasone, or hydrocortisone were comparable with that of control, showing diameters (DM) of 160 ± 8, 156 ± 6, and 159 ± 7 μm, respectively (Figure S4A). Budesonide-treated aggregates displayed a similar spheroidal morphology but were smaller in size compared with controls (budesonide 121 ± 6 μm versus control 157 ± 6 μm) (Figure S4A). Unlike budesonide, dexamethasone-, fluticasone-, and hydrocortisone-treated gastruloids all displayed a polarized morphology at 120 h (EI > 2.0), independently of the duration of the treatment (Figure 3C), and elongated with a similar timing compared with controls (Figures S4B and S4C). To assess whether higher doses of the glucocorticoids might affect gastruloid development, we analyzed the effect of the different drugs at 20 and 40 μM (Figure S4D). Dexamethasone, fluticasone, and hydrocortisone did not affect gastruloid development even at the highest concentrations, as confirmed by the polarized expression of CDX2 (Figures S4D and S4E).

We thus assessed if dexamethasone was able to counteract the effect of budesonide by treating gastruloids with both dexamethasone and budesonide at the same concentration (10 μM). The diameter of the aggregates (48 h) treated with the combination of budesonide and dexamethasone was comparable with that of budesonide alone (Figure S4A), suggesting that dexamethasone was unable to counteract the inhibitory effect of budesonide. To further address this issue, we performed a dose-response analysis using dexamethasone at concentrations ranging from 10 to 40 μM in combination with budesonide (10 μM). The aggregates treated with a combination of budesonide + dexamethasone maintained a spherical morphology at 120 h (EI ∼ 1) and failed to express the A-P marker BRACHYURY (Figure S4F), thus indicating that dexamethasone was unable to counteract the inhibitory effect of budesonide even at the highest concentrations.

Of note, while long-term (0–120 h) budesonide treatment resulted in tiny, round-shaped cell aggregates that did not elongate, transient (0–48 h) exposure to budesonide resulted in aggregates that started to expand (DM = 212 ± 14 versus 280 ± 23 μm) (Figure 3D), thus excluding any toxic effects of budesonide treatment. To assess whether transient (0–48 h) exposure to budesonide might delay gastruloid development, gastruloid cultures were extended to 168 h. Interestingly, a percentage of gastruloids (6/30) elongated and induced polarized expression of BRACHYURY at 168 h (Figure 3E), suggesting that budesonide withdrawal allows, at least in part, the recovery of the gastruloid development process.

All together these data indicate that the inhibitory effect of budesonide is independent of its glucocorticoid activity, and is reversible (Figure 3F).

## Budesonide-dependent inhibition of esMT and gastruloid development does not rely on the GR

Budesonide is classified as an agonist of the GR/nuclear receptor subfamily 3 group C member 1 (GR/NR3C1) (DrugBank/DB01222; CHEMBL1370). To investigate whether the inhibitory effects of budesonide rely on GR, we assessed the effect of *Nr3c1* silencing. To this end, ESCs were infected with lentiviral particles carrying short hairpin RNA (shRNA) molecules targeting either different regions of *Nr3c1* gene transcript (*Nr3c1*-shRNA#1, shRNA#2, and shRNA#3) or non-targeting control shRNAs (shNT) (Figure 4). Efficient *Nr3c1* downregulation (up to 90%) was confirmed at both RNA and protein levels (Figure 4A).

*Nr3c1* knockdown (KD) cells were fully able to undergo esMT in response to a high-proline regimen (Figure 4B). Moreover, budesonide reduced the fraction of irregular/flat-shaped colonies and increased the fraction of domed-shaped colonies to a similar extent in proline-treated *Nr3c1* KD and NT ESCs (Figure 4B). These data suggested that the GR/glucocorticoid pathway is dispensable both for esMT induction and budesonide-dependent inhibition of esMT.

To further explore the role of the GR pathway in budesonide-dependent inhibition of gastruloid development, we evaluated the ability of *Nr3c1* KD cells to generate gastruloids. At 48 h after seeding, budesonide-treated NT and *Nr3c1* KD aggregates exhibited a compacted spherical shape and were smaller in size compared with untreated aggregates (∼130 versus ∼170 μm) (Figure 4C), suggesting that budesonide induced cell aggregate compaction in an *Nr3c1*-independent manner. Furthermore, budesonide-treated NT and *Nr3c1* KD aggregates both maintained a round-shaped morphology at 120 h (Figure 4C), suggesting that the inhibitory effect of budesonide does not depend on GR. To corroborate this hypothesis, we tested the effect of relacorilant (PubChem CID:73051463), a nonsteroidal selective GR antagonist (Hunt et al., 2017) on gastruloid

(B) Boxplot diagram showing the fraction (%) of irregular/flat colonies (left), and representative bright-field images (right) of control (shNT) and *Nr3c1*KD colonies from FBS/LIF ESCs ± proline (500 μM) ± budesonide (10 μM; n = 3; 20 fields/condition). Scale bar, 200 μm.
(C) Boxplot diagram of the diameter (left) and representative bright-field images (right) of control (shNT) and *Nr3c1*KD ESCs ± budesonide-derived aggregates at 48 and 120 h (n = 3; 21 aggregates/condition). Scale bar, 100 μm.
(D) Representative bright-field images of cell aggregates (48 h) and gastruloids (120 h) treated with budesonide or relacolirant at the indicated concentrations. Scale bar, 50 μm.
(E) Schematic representation of the effect of budesonide on esMT and gastruloid development of *Nr3c1*KD cells.

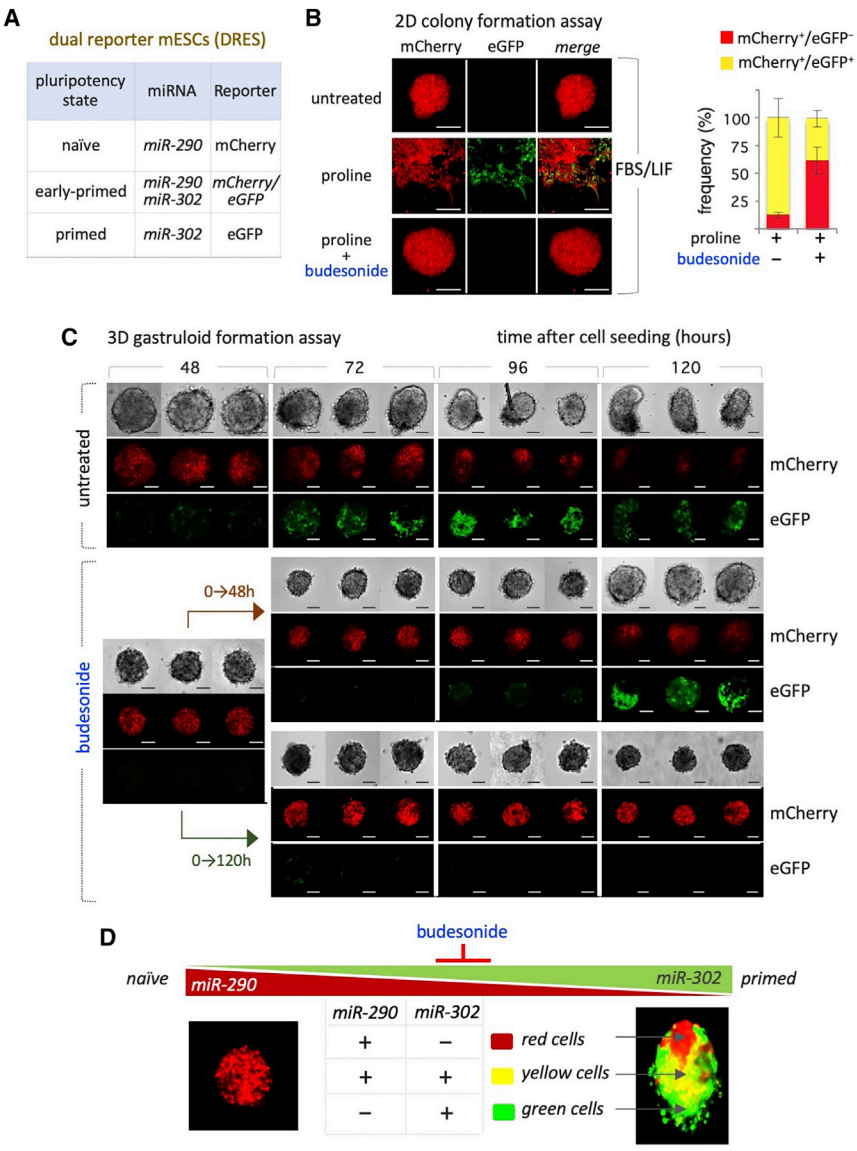


**Figure 5. Budesonide prevents miR-290 to miR-302 molecular switch**

(A) Schematic expression of miR-290/mCherry and miR-302/GFP from dual reporter ESCs (DRES) in different pluripotency states.

(B) Representative confocal images (left) of FBS/LIF DRES ± proline (500 μM) ± budesonide (10 μM) colonies at 120 h (300 cells/cm$^2$). Scale bar, 100 μm. FACS-based quantification (%) of mCherry$^+$/eGFP$^-$ (red) and mCherry$^+$/eGFP$^+$ (yellow) cells in FBS/LIF DRES + proline (500 μM) ± budesonide (10 μM).

(C) Representative confocal images of mCherry and eGFP expression and bright-field images of DRES-derived gastruloids ± budesonide (10 μM) for 0–48 h (orange brown arrow) and 0–120 h (green arrow) at the indicated time points. Scale bar, 50 μm.

(D) Budesonide prevents miR-290 to miR-302 molecular switch (top) and 3D fluorescent images (bottom) of untreated (right) and budesonide-treated (left) DRES gastruloids.

formation. In line with our hypothesis, unlike budesonide, transient treatment (0–48 h) of wild-type aggregates with relacorilant (10 μM) did not affect gastruloid elongation (Figure 4D). However, when relacorilant was supplemented at 40 μM the aggregates appeared tiny and largely surrounded by cell debris (Figure 4D), indicating a toxic effect of the drug at this concentration.

Taken together, these data support the idea that budesonide prevents gastruloid elongation through a glucocorticoid pathway-independent mechanism (Figure 4E).

## Budesonide counteracts exit from pluripotency in 3D ESC aggregates

To get insights into the molecular events mediating budesonide effects on gastruloid development, we first analyzed the transition from pluripotency toward differentiation. To this end, we used the dual reporter embryonic stem cells (DRES) to follow the naive to primed pluripotency transition based on the expression of reporters for miR-290 (E3.5–E6.75; mCherry) and miR-302 (E4.75–E8.0; eGFP) loci (Figure 5A) (Parchem et al., 2014). As described previously (D'Aniello et al., 2017), FBS/LIF-cultured DRES generated round-shaped colonies mostly positive to miR-290-mCherry; upon proline supplementation, the cells grew as flat irregular colonies and the miR-302-eGFP expression was induced (Figure 5B). Addition of budesonide inhibited both the phenotypic (domed-to-flat) transition and the molecular (miR-290 to miR-302) switch (Figure 5B), suggesting that budesonide prevents proline-induced exit from pluripotency in 2D culture.

We thus assessed the effect of either short- or long-term budesonide treatment on DRES-derived 3D gastruloids. Time-course analysis of mCherry/eGFP expression showed that, 48 h after seeding, control/untreated aggregates were mostly positive to miR-290-mCherry expression, while from 72 h onward the expression of miR-302-eGFP progressively increased as the elongation proceeded, concomitant to the downregulation of miR-290-mCherry (Figure 5C). Following short treatment (0–48 h) with budesonide, DRES aggregates maintained a strong miR-290-mCherry expression up to 96 h after seeding, while induction of miR-302-eGFP expression was delayed, being clearly detectable only at 120 h compared with control aggregates. This expression profile correlated with the morphological changes observed in the 0–48 h budesonide-treated aggregates, which showed a round-shaped morphology up to 96 h, and started to become ovoidal/to elongate at 120 h (Figure 5C). These results support the notion that the inhibitory effect of budesonide is reversible (Figure 3E). Conversely, upon long-term (0–120 h) treatment with budesonide, DRES aggregates almost exclusively expressed miR-290-mCherry, while miR-302-eGFP expression was undetectable, and the aggregates maintained a compacted round-shaped morphology (Figures 5C and 5D).

To investigate this further, we analyzed E-CADHERIN localization and compared the genome-wide expression profile of control and budesonide-treated 3D aggregates soon after CHIR supplementation (80 h) (Figure 6A). Despite the fact that E-CADHERIN was similarly localized in the intercellular space in both control and budesonide-treated aggregates, the principal component analysis (PCA) revealed significant differences between the two transcriptional profiles with ~1,700 differentially regulated genes (fold change $\geq 1.5$; padj $< 0.05$) (Figure 6A; Table S1). Gene ontology analysis unveiled a significant enrichment in terms related to multicellular organism development, antero-posterior pattern specification, and locomotion (Figure 6B). Furthermore, while naive pluripotency genes (*Esrrb*, *Nr0b1*, *Pecam1*, *Prdm14*, *Tfcp2l1*, and *Rex1/Zfp42*) were expressed at higher levels in budesonide-treated gastruloids, primed pluripotency (*Cer1*, *Dnmt3b*, and *Lin28*) and differentiation markers (*Brachyury*, *Epha1*, *Fgf8*, *Lefty1*, *Nes*, *Nkx1,2*, and *Wnt8a*) showed the opposite trend (Table S1; Figures 6C and 6D). Interestingly, budesonide altered the expression of genes involved in WNT signaling, which plays a key role in symmetry breaking (Turner et al., 2016), suggesting that budesonide interfere with the differentiation process.

To explore this hypothesis, we first analyzed the expression profile of pluripotency and differentiation markers on control and budesonide-treated gastruloids at 120 h (Figure 6E). As expected, only a few cells of properly elongated control aggregates showed detectable levels of OCT4 and NANOG pluripotency markers. Conversely, budesonide-treated (0–48 and 0–120 h) spherical aggregates were mostly enriched in $OCT4^+$, $NANOG^+$, and $SOX2^+$ cells, with $NANOG^+$ cells located preferentially at the center of the cell aggregates (Figure 6E). Furthermore, control gastruloids exhibited a polarized expression of both BRACHYURY and CDX2, which, conversely, was almost undetectable in budesonide-treated (0–120 h) aggregates (Figure 6E). In line with the idea of a reversible inhibitory effect of budesonide, BRACHYURY and CDX2 were induced in short-term (0–48 h) budesonide-treated aggregates (Figure 6E). Furthermore, unlike control gastruloids, budesonide-treated cell aggregates at 120 h maintained high levels of E-CADHERIN expression at the cell-cell interface (Figure 6F).

Finally, we determined whether persistent expression of pluripotency genes and downregulation of differentiation markers translate to increased self-renewal of budesonide-treated aggregates. To address this issue, both control and budesonide-treated gastruloids at 120 h were dissociated and the cells plated at low density (150 cells/$cm^2$) in FBS/2i/LIF medium; the resulting colonies were quantified and stained with alkaline phosphatase (ALP) (Figure S5A). Cells derived from control elongated gastruloids gave rise to a few domed-shaped, ALP-positive colonies; this fraction strongly increased (~10-fold) in the cell population derived from budesonide-treated aggregates (Figure S5B).

All together these data provide molecular and functional evidence that budesonide locks 3D cell aggregates in a naive state preventing symmetry breaking and AP specification, and suggest that this may occur through promotion of cell-cell adhesion/compaction and inhibition of cellular locomotion processes (Figure 6G).

## Budesonide forces epithelial-like cell-cell junctions in 2D conditions

To further test the hypothesis that budesonide prevents differentiation maintaining cell-cell adhesion, we analyzed the impact of budesonide on 2D ESCs under different culture conditions. First, we analyzed the effect of budesonide on ESCs cultured in FBS/LIF (Figure S6A). As expected, FBS/LIF ESC populations showed a heterogeneous phenotype, with a fraction (10% ± 5%) of colonies exhibiting an irregular/flat morphology (Figure S6B). This phenotypic heterogeneity was less pronounced in the presence of budesonide, resembling that of ESCs cultured in 2i/LIF (Figures S6B and S6C). Of note, this correlated with different subcellular localization of E-CADHERIN protein. Indeed, while in the round-shaped colonies E-CADHERIN was enriched at the cell-cell contacts, it was delocalized to the perinuclear regions of cells located at the periphery of the flat-shaped colonies (Figure 7A). Furthermore, budesonide significantly reduced the fraction of NANOG negative

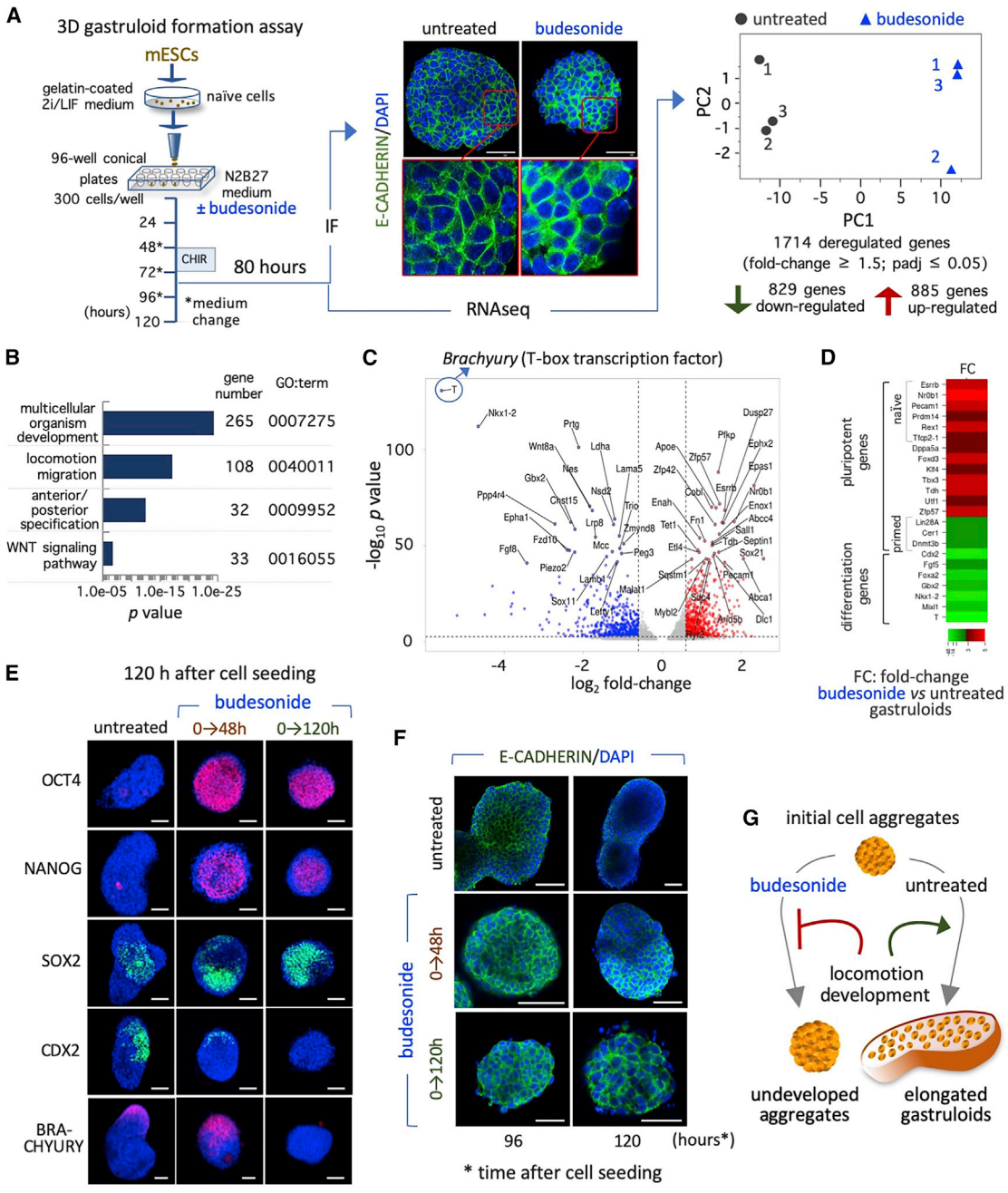


**Figure 6. Budesonide prevents differentiation and maintains the pluripotency transcription program in 3D cell aggregates**

(A) Schematic representation of the experimental design (left) and representative confocal images (middle) of E-CADHERIN in gastruloids ± budesonide. Nuclei were counterstained with DAPI (blue). Scale bar, 50 μm. Principal-component analysis (PCA) of control (untreated) and budesonide-treated (80 h) gastruloid expression profiles (right).

(B) Gene ontology analysis of deregulated genes in budesonide-treated gastruloids.

(C) Volcano plot showing downregulated (blue) and upregulated (red) genes in budesonide-treated versus untreated gastruloids.

(D) Fold change heatmap of pluripotency (naive and primed) and differentiation genes in budesonide-treated versus untreated gastruloids.

(E) Representative confocal images of OCT4, NANOG, BRACHYURY (red), SOX2, and CDX2 (green) expression in gastruloids ± budesonide for 0–48 h (orange brown arrow) and 0–120 h (green arrow). Nuclei were counterstained with DAPI. Scale bar, 50 μm.

(F) Representative confocal images of E-CADHERIN in gastruloids ± budesonide for 0–48 h (orange brown arrow) and 0–120 h (green arrow) at 120 h. Nuclei were counterstained with DAPI. Scale bar, 50 μm.

(G) Schematic representation of the effect of budesonide on cell aggregates. See also Figure S5.

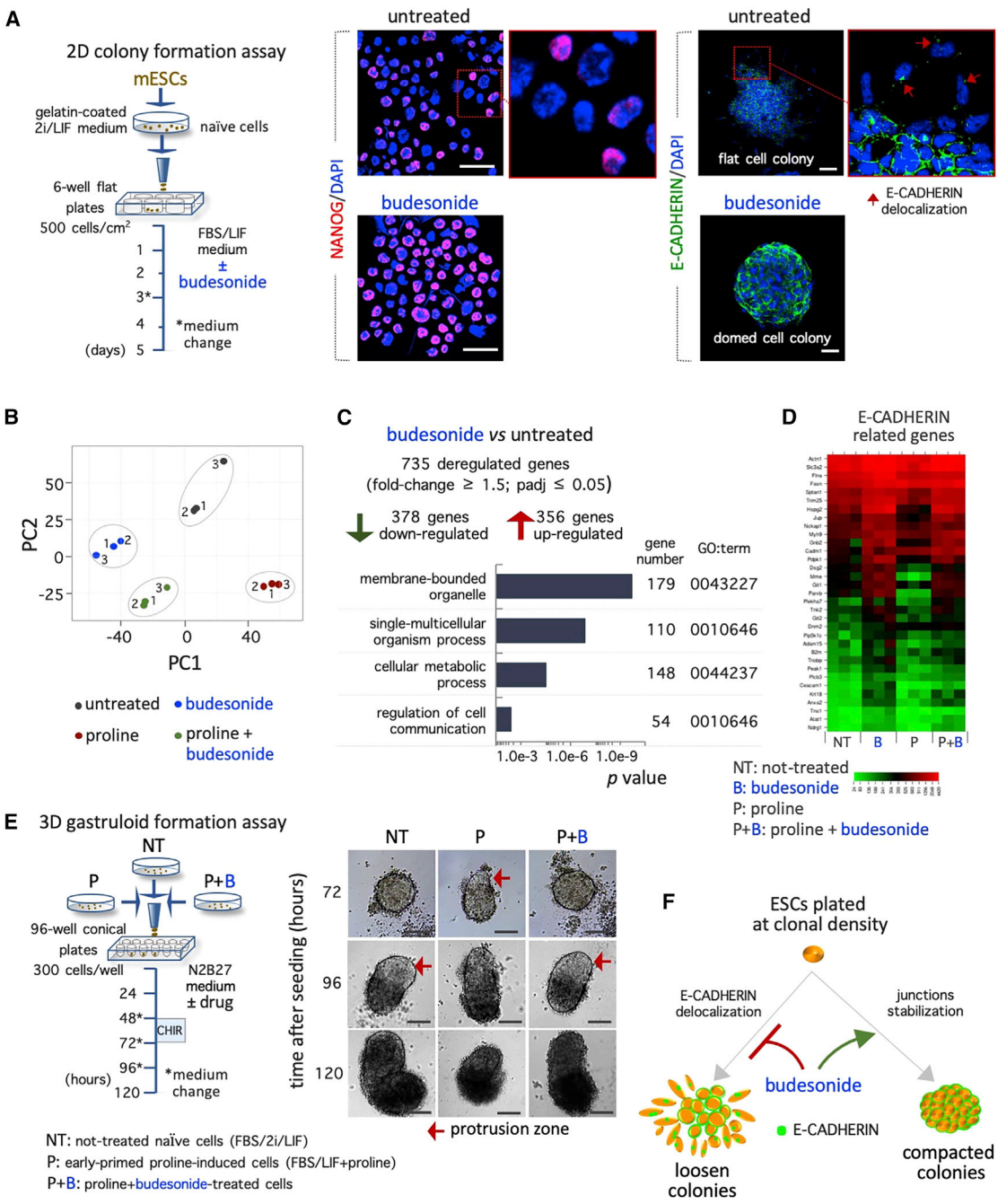


**Figure 7. Budesonide maintains naive pluripotency in 2D cell aggregates**

(A) Schematic representation of the assay (left) and representative confocal images of NANOG (red) and E-CADHERIN (green) expression on colonies (right) and cytospin preparation (middle) from FBS/LIF ESCs ± budesonide (10 μM). Scale bars, 100 and 50 μm. Red arrows indicate E-CADHERIN delocalization in cells at the border of flat colonies. Nuclei were counterstained with DAPI (blue).

(B) PCA of the expression profiles of FBS/LIF ESCs ± proline (500 μM) ± budesonide (10 μM) at 72 h.

(C) Gene ontology analysis of deregulated genes in budesonide-treated versus untreated cells.

(D) Heatmaps showing the expression levels of E-CADHERIN-related genes in FBS/LIF ESCs ± proline (500 μM) ± budesonide (10 μM).

(E) Schematic representation of gastruloid formation assay (left) and representative bright-field images (right) of gastruloids from FBS/LIF ESCs treated with either proline alone (500 μM; P) or proline + budesonide (10 μM; P+B) or FBS/2i/LIF ESCs (NT). Scale bar, 100 μm.

(F) Schematic representation the effect of budesonide on E-CADHERIN localization and colonies morphology. See also Figure S6.

cells in FBS/LIF ESC cultures, similar to that observed upon addition of CHIR99021and PD0325901 either alone or in combination (2i) (Figures 7A, S6B, and S6C), suggesting that budesonide reduces the phenotypic and molecular heterogeneity of FBS/LIF ESCs.

We then tested the effect of budesonide on spontaneous ESC differentiation triggered by 2i/LIF withdrawal. To this aim, ESCs were cultured in FBS/2i/LIF for 3 days and then either shifted to a medium containing FBS ± budesonide or maintained in FBS/2i/LIF as a control (time 0), and the colony morphology was analyzed over time up to 96 h (Figure S6D). As expected, while FBS/2i/LIF ESCs colonies were tightly packed and maintained an undifferentiated morphology, the majority of FBS ESC colonies exhibited a flat-shaped morphology and appeared differentiated (∼80% at 96 h) (Figure S6E). Accordingly, the percentage of NANOG-positive cells strongly decreased in FBS compared with FBS/2i/LIF culture (66.8 ± 3.3 2i/LIF versus 7.1 ± 0.7 FBS) (Figure S6F). Addition of budesonide to FBS culture medium strongly reduced the fraction of flat colonies from ∼80% to ∼30% and increased that of NANOG-positive cells (7.1 ± 0.7 FBS versus 39.4 ± 4.8 FBS + budesonide) (Figure S6F), suggesting that exit from pluripotency is significantly delayed in the presence of budesonide.

We thus went on and assessed the effect of budesonide in conditions that induce exit from naive pluripotency, namely proline supplementation to FBS/LIF ESCs (Comes et al., 2013; D'Aniello et al., 2017), analyzing the transcriptome profile of FBS/LIF ESCs ± proline ± budesonide. Budesonide induced a significant variation in the transcriptome of both naive (FBS/LIF) and early primed (FBS/LIF + proline) cells (Table S2). PCA placed proline + budesonide-treated cells between FBS/LIF and FBS/LIF + budesonide ESCs (Figure 7B), providing molecular support to the morphological analysis (Figures 3A and S5B). Of note, budesonide preserved the expression of genes associated with naive pluripotency, such as *Esrrb*, *Pecam1*, *Rex1/Zfp42*, and *Tfcp2l1*, and prevented the upregulation of primed pluripotency markers (*Dnmt3b*, *Lin28*, and *Otx2*) in FBS/LIF + proline culture conditions (Table S2). Gene ontology analysis of DRGs (∼700 in FBS/LIF ESCs ± budesonide; fold change $\geq 1.5$; padj <0.05) (Table S2) revealed significant enrichment of terms related to regulation of cell communication, cellular metabolic process, and membrane-bounded organelles (Figure 7C). Furthermore, budesonide altered the expression of a large set of genes involved in E-CADHERIN stabilization (Figure 7D), supporting the idea that it promotes cell-cell communication. Finally, to investigate the functional features of proline + budesonide-treated cells, we assessed their gastruloid formation competence (Figure 7E). While, as expected, PiCs developed gastruloids that elongated earlier and were smaller in size compared with naive ESC-derived gastruloids (Cermola et al., 2021), proline + budesonide-treated cells generated gastruloids comparable with those of naive ESCs (Figure 7E), thus providing further evidence that budesonide counteracts the effect of proline and favors features of naive pluripotency.

All together, these results support and extend our findings on 3D gastruloids and indicate that budesonide maintains an epithelial-like phenotype counteracting the differentiation stimuli also in 2D conditions (Figure 7F).

## DISCUSSION

Here, we interrogated the mechanism(s) that triggers symmetry breaking in pluripotent stem cells using a chemical genetic approach. Our findings revealed that budesonide, a glucocorticoid widely used to treat airways and gastrointestinal syndromes, including asthma, Crohn disease, and ulcerative colitis (Kalola and Ambati, 2021), enables ESCs to withstand differentiation stimuli and prevents spontaneous symmetry breaking in mouse 3D gastruloids. Budesonide activity is so far attributed to its glucocorticoids' anti-inflammatory activity; here, we demonstrate that the inhibitory effect of budesonide is independent from the GR. Complementary to the findings that *Nr3c1*/GR silencing does not affect gastruloid formation, we show that none of the classical GR agonists or antagonists, including dexamethasone, fluticasone, hydrocortisone, and relacorilant, a nonsteroidal selective GR antagonist, prevents gastruloid development. Of note, GR-independent "non-genomic" effects of glucocorticoids have been described, which hinge on nonspecific interactions of steroidal molecules with cellular membranes (Losel et al., 2003). Although we cannot rule out this mechanism, this would not explain why budesonide but not the structurally related dexamethasone, fluticasone, and hydrocortisone inhibits the self-organization process of ESCs. Furthermore, it is well known that glucocorticoids mainly promote GR-mediated differentiation in different cellular context (Hartmann et al., 2016); conversely, budesonide counteracts exit from pluripotency under conditions of either spontaneous or induced differentiation. Of note, unlike budesonide, none of the other recently identified inhibitors of esMT, i.e., propafenone and spiramycin belonging to different chemical classes, (D'Aniello et al., 2019), interferes with gastruloid elongation, further confirming the specificity of budesonide activity.

Different lines of evidence indicate that budesonide promotes cell-cell adhesion both in 2D and 3D conditions and suggest that this eventually halts cell fate transition. First, budesonide reduces the spontaneous phenotypic and molecular heterogeneity of FBS/LIF ESC population and

prevents exit from pluripotency under different conditions, including LIF withdrawal and addition of proline to FBS/LIF ESCs. Similarly, budesonide maintains highly compacted floating aggregates of ESCs and impedes exit from pluripotency under conditions that induce 3D gastruloid formation. Of note, budesonide-dependent inhibition of gastruloid development is reversible as removal of budesonide from cell aggregates at 48 h rescues, at least in part, the aberrant phenotype and results in aggregates that elongate and express the differentiation markers.

A role of cell tension in regulating cell fate specification in early development has been uncovered in human ESCs. Indeed, high cell-adhesion tension promotes mesoderm specification and emergence of gastrulation-like nodes, which relies on the phosphorylation-dependent release of β-catenin from junctions and its nuclear translocation (Muncie et al., 2020). Furthermore, disruption of epithelial integrity has been reported to promote mesendoderm differentiation by increasing sensitiveness to morphogens (Rattier et al., 2021). In 3D gastruloids, pharmacological activation of WNT signaling through a pulse of CHIR99021 induces a break-down of the E-CADHERIN-mediated cell-cell contacts and promotes collective cell migration; conversely, in the absence of WNT activation, E-CADHERIN expression is maintained and the aggregates retain a spheroidal shape (Hashmi et al., 2021). Here, we demonstrate that budesonide maintains E-CADHERIN at the cell membrane and alters the expression of genes involved in WNT signaling, blocking gastruloid development. Mechanistically, we show that budesonide does not counteract, at least in our conditions, the inductive effect of CHIR9902. This is also supported by the fact that, while CHIR99021 either promotes (3D gastruloids) or prevents (esMT) ESC differentiation, budesonide inhibits both 3D gastruloids and esMT, suggesting a different mechanism of action.

Although further studies are necessary to clarify the mechanism, our findings lead to the hypothesis that budesonide prevents symmetry breaking of ESC aggregates at least in part by interfering with the E-CADHERIN-β-CATENIN/WNT axis. It is well known that E-CADHERIN adhesive protein is essential to preserve both aggregation/compaction propensity and naive pluripotency of ESCs (Larue et al., 1994; Pieters and van Roy, 2014; Redmer et al., 2011; Riethmacher et al., 1995); yet, the relationship between exit from naive pluripotency and reprograming of the cell-cell interactions is still debated. Here, we propose that budesonide-dependent maintenance of cell-cell adhesion shields ESCs from the differentiation signals in 2D and 3D conditions, and locks cells in pluripotency preventing symmetry breaking in 3D gastruloids.

Gastruloids have been recently proposed as cell-based models for drug safety testing (Mantziou et al., 2021); our findings showing that a commonly used antiasthma drug inhibits gastruloid development, can open the way to further investigate unwanted effects of budesonide treatment on fertility in women. Indeed, partial infertility has been reported in asthmatic women (Gade et al., 2014; Vejen Hansen et al., 2019), yet, to our knowledge, the effects of budesonide on pregnancy have not been directly investigated with well-controlled and adequate clinical trials (Kalola and Ambati, 2021). This could be highly relevant also in light of the fact that budesonide has recently emerged as a promising drug candidate to treat COVID-19 (Heinen et al., 2021; Konduri et al., 2021; Ramakrishnan et al., 2021; Yu et al., 2021). Of note, it is known that budesonide, unlike the glucocorticoids beclomethasone, prednisolone, dexamethasone, and betamethasone, cannot be metabolized by the placental enzyme 11β-hydroxysteroid dehydrogenase type 2 (Murphy et al., 2007).

In conclusion, our data provide evidence that budesonide locks pluripotent stem cells in an epithelial-like state and support the idea that cell-cell adhesion properties regulate symmetry breaking and cell fate transition. Furthermore, our findings strongly support the idea that gastruloids can be successfully used to uncover previously unidentified adverse effects of drugs on embryo development.

## EXPERIMENTAL PROCEDURES

### ESC culture conditions and PiC generation

Wild-type E14Tg2a (E14) and DRES ESCs (Parchem et al., 2014) were grown in FBS/LIF as described previously (D'Aniello et al., 2017; Fiorenzano et al., 2016). The cell lines were routinely tested and confirmed to be free of mycoplasma. PiCs were obtained from naive ESCs as described previously (Comes et al., 2013). Crystal violet staining and colony type analysis were performed as described (Comes et al., 2013).

### Gastruloid formation

Gastruloid formation assay was performed as described (Cermola et al., 2021, 2022). ESCs were seeded at 2.5–3.0 × $10^2$ cells/well, except for DRES (6 × $10^2$ cells/well). See supplemental information for details. Morphometric analysis of gastruloids was performed using ImageJ 1.46r software (https://imagej.nih.gov/ij/). Elongation index was calculated using ImageJ-Fiji (BIOP plugin).

### Proliferation and apoptosis assays

ESCs were plated at 15,000 cells/$cm^2$ ± indicated drugs. Proliferation was evaluated using Click-iT EdU Flow Cytometry (Molecular Probes) assay, following the manufacturer's instructions. ESCs were incubated ON at 37°C with EdU (10 μM) and analyzed using FACSARIAIII (Becton Dickinson). Apoptosis was evaluated using Annexin V/propidium iodide assay (Dojindo Laboratories) and

analyzed by FACS using the Diva software (BD Biosciences, San Jose, CA).

### RNA extraction and quantitative real-time PCR

Total RNAs were isolated using either the RNeasy kit or Trizol (Invitrogen) and reverse transcribed using QuantiTect Reverse Transcription kit (QIAGEN). Quantitative real-time PCR was performed using SYBR Green PCR master mix (FluoCycle II SYBR, EuroClone). Primers are listed in Table S4.

### RNA sequencing analysis

3′ RNA sequencing was performed at Genomix4Life S.r.l. using the Illumina platform. Raw data were aligned to Genecode M27 (GRCm39). Quantification of gene expression was performed using FeatureCounts (version 2.0). R software was used to create a matrix of all genes expressed in all samples with the corresponding read-counts, and Bioconductor package DESeq2 was used to normalize the data, using the median of ratio to perform differential expression analysis ($p < 0.05$). In particular, the counts were divided by sample-specific size factors determined by median ratio of gene counts relative to geometric mean per gene.

### Immunofluorescence and western blot

Immunofluorescence on gastruloids was performed as described (Baillie-Johnson et al., 2015; Cermola et al., 2021). For staining with BRACHYURY, gastruloids were washed at RT with PBS (3×, 10 min), PBS/10% FBS/0.5% Triton X-PBSFT (1×, 10 min), and with PBSFT (1 h, 4°C), and incubated with antibodies (48 h, at 4°C) on a low-speed orbital rocker. Confocal images were obtained on a Nikon A1 microscope. The AF6000 (Leica Microsystems) and NIS Element C (Nikon, Tokyo) software were used for image acquisition/elaboration.

Western blot analysis was performed as described (D'Aniello et al., 2017). See supplemental experimental procedures for details. Primary and secondary antibodies are listed in Table S3.

### Quantification and statistical analysis

The number of independent experiments is reported as "*n*" in the caption of each figure and the total samples size is indicated. Statistical significance was determined by a two-tailed paired Student's t test. Results are presented as the mean ± SD (standard deviation of the mean) or as box/dot plot displaying minimum, first quartile, median, third quartile, and maximum. Box/dot plots were generated using RStudio software (https://www.rstudio.com/) v.1.1.463.

### Accession numbers

The accession number for RNA-seq data reported in this paper is GEO: GSE199767.

## SUPPLEMENTAL INFORMATION

Supplemental information can be found online at https://doi.org/10.1016/j.stemcr.2022.09.013.

## AUTHOR CONTRIBUTIONS

F.C., F.A., C.D'A., E.J.P. and G.M. conceived and designed the study. F.C., F.A., F.S., E.I., A.F., G.C., C.D'A., D.D.C., and E.J.P. performed the experiments. F.C. performed statistical analysis. E.S. and C.C. gave conceptual advice. D.D.C., A.F., and G.C. contribute to the editing of the manuscript. E.J.P. and G.M. wrote the manuscript.

## ACKNOWLEDGMENTS

We are grateful to Salvatore Arbucci and members of the Integrated Microscopy and FACS Facilities of IGB-ABT, CNR. We thank Gennaro Andolfi for excellent technical assistance. We are grateful to Ombretta Guardiola for helpful discussions. This study was supported by Associazione Italiana per la Ricerca sul Cancro AIRC (grant IG 20736), Italian Ministry of Education-University-Research (CTN01_00177; PRIN 2017XJ38A4).

## CONFLICT OF INTERESTS

E.S. and C.C. are employees of Chiesi Farmaceutici S.p.A.

Received: April 1, 2022
Revised: September 26, 2022
Accepted: September 27, 2022
Published: October 27, 2022

## REFERENCES

Baillie-Johnson, P., van den Brink, S.C., Balayo, T., Turner, D.A., and Martinez Arias, A. (2015). Generation of aggregates of mouse embryonic stem cells that show symmetry breaking, polarization and emergent collective behaviour in vitro. J. Vis. Exp., 53252. https://doi.org/10.3791/53252.

Casalino, L., Comes, S., Lambazzi, G., De Stefano, B., Filosa, S., De Falco, S., De Cesare, D., Minchiotti, G., and Patriarca, E.J. (2011). Control of embryonic stem cell metastability by L-proline catabolism. J. Mol. Cell Biol. *3*, 108–122. https://doi.org/10.1093/jmcb/mjr001.

Cermola, F., D'Aniello, C., Tatè, R., De Cesare, D., Martinez-Arias, A., Minchiotti, G., and Patriarca, E.J. (2021). Gastruloid development competence discriminates different states of pluripotency. Stem Cell Rep. *16*, 354–369. https://doi.org/10.1016/j.stemcr.2020.12.013.

Cermola, F., Patriarca, E.J., and Minchiotti, G. (2022). Generation of gastruloids from epiblast-like cells. Methods Mol. Biol. *2490*, 197–204. https://doi.org/10.1007/978-1-0716-2281-0_14.

Comes, S., Gagliardi, M., Laprano, N., Fico, A., Cimmino, A., Palamidessi, A., De Cesare, D., De Falco, S., Angelini, C., Scita, G., et al. (2013). L-Proline induces a mesenchymal-like invasive program in embryonic stem cells by remodeling H3K9 and H3K36 methylation. Stem Cell Rep. *1*, 307–321. https://doi.org/10.1016/j.stemcr.2013.09.001.

D'Aniello, C., Cermola, F., Palamidessi, A., Wanderlingh, L.G., Gagliardi, M., Migliaccio, A., Varrone, F., Casalino, L., Matarazzo, M.R., De Cesare, D., et al. (2019). Collagen prolyl hydroxylation-dependent metabolic perturbation governs epigenetic remodeling and mesenchymal transition in pluripotent and cancer cells.

Cancer Res. *79*, 3235–3250. https://doi.org/10.1158/0008-5472.CAN-18-2070.

D'Aniello, C., Fico, A., Casalino, L., Guardiola, O., Di Napoli, G., Cermola, F., De Cesare, D., Tatè, R., Cobellis, G., Patriarca, E.J., and Minchiotti, G. (2015). A novel autoregulatory loop between the Gcn2-Atf4 pathway and (L)-Proline [corrected] metabolism controls stem cell identity. Cell Death Differ. *22*, 1094–1105. https://doi.org/10.1038/cdd.2015.24.

D'Aniello, C., Habibi, E., Cermola, F., Paris, D., Russo, F., Fiorenzano, A., Di Napoli, G., Melck, D.J., Cobellis, G., Angelini, C., et al. (2017). Vitamin C and l-proline antagonistic effects capture alternative states in the pluripotency continuum. Stem Cell Rep. *8*, 1–10. https://doi.org/10.1016/j.stemcr.2016.11.011.

Fiorenzano, A., Pascale, E., D'Aniello, C., Acampora, D., Bassalert, C., Russo, F., Andolfi, G., Biffoni, M., Francescangeli, F., Zeuner, A., et al. (2016). Cripto is essential to capture mouse epiblast stem cell and human embryonic stem cell pluripotency. Nat. Commun. *7*, 12589. https://doi.org/10.1038/ncomms12589.

Gade, E.J., Thomsen, S.F., Lindenberg, S., Kyvik, K.O., Lieberoth, S., and Backer, V. (2014). Asthma affects time to pregnancy and fertility: a register-based twin study. Eur. Respir. J. *43*, 1077–1085. https://doi.org/10.1183/09031936.00148713.

Hartmann, K., Koenen, M., Schauer, S., Wittig-Blaich, S., Ahmad, M., Baschant, U., and Tuckermann, J.P. (2016). Molecular actions of glucocorticoids in cartilage and bone during health, disease, and steroid therapy. Physiol. Rev. *96*, 409–447. https://doi.org/10.1152/physrev.00011.2015.

Hashmi, A., Tlili, S., Perrin, P., Martinez-Arias, A., and Lenne, P.-F. (2021). Cell-state transitions and collective cell movement generate an endoderm-like region in gastruloids. Preprint at bioRxiv. https://doi.org/10.1101/2020.05.21.105551.

Heinen, N., Meister, T.L., Klohn, M., Steinmann, E., Todt, D., and Pfaender, S. (2021). Antiviral effect of budesonide against SARS-CoV-2. Viruses *13*, 1411. https://doi.org/10.3390/v13071411.

Hunt, H.J., Belanoff, J.K., Walters, I., Gourdet, B., Thomas, J., Barton, N., Unitt, J., Phillips, T., Swift, D., and Eaton, E. (2017). Identification of the Clinical Candidate (R)-(1-(4-Fluorophenyl)-6-((1-methyl-1H-pyrazol-4-yl)sulfonyl)-4, 4a, 5, 6, 7, 8-hexah ydro-1H-pyrazolo[3, 4-g]isoquinolin-4a-yl)(4-(trifluoromethyl) pyridin-2-yl)methano ne (CORT125134): a Selective Glucocorticoid Receptor (GR) Antagonist. J. Med. Chem. *60*, 3405–3421. https://doi.org/10.1021/acs.jmedchem.7b00162.

Kalola, U.K., and Ambati, S. (2021). Budesonide. In StatPearls.

Kawasumi, M., and Nghiem, P. (2007). Chemical genetics: elucidating biological systems with small-molecule compounds. J. Invest. Dermatol. *127*, 1577–1584. https://doi.org/10.1038/sj.jid.5700853.

Konduri, K.S., Pattisapu, R., Pattisapu, J., Konduri, G.G., Zwetchkenbaum, J., Roy, B., Barman, M., Frazier, A., Hurst, B.L., and Düzgüneş, N. (2021). ProLung-budesonide inhibits SARS-CoV-2 replication and reduces lung inflammation. Arch. Pharmacol. Ther. *3*, 52–65. https://doi.org/10.33696/pharmacol.3.028.

Larue, L., Ohsugi, M., Hirchenhain, J., and Kemler, R. (1994). E-cadherin null mutant embryos fail to form a trophectoderm epithelium. Proc. Natl. Acad. Sci. USA *91*, 8263–8267. https://doi.org/10.1073/pnas.91.17.8263.

Losel, R.M., Falkenstein, E., Feuring, M., Schultz, A., Tillmann, H.C., Rossol-Haseroth, K., and Wehling, M. (2003). Nongenomic steroid action: controversies, questions, and answers. Physiol. Rev. *83*, 965–1016. https://doi.org/10.1152/physrev.00003.2003.

Mantziou, V., Baillie-Benson, P., Jaklin, M., Kustermann, S., Arias, A.M., and Moris, N. (2021). In vitro teratogenicity testing using a 3D, embryo-like gastruloid system. Reprod. Toxicol. *105*, 72–90. https://doi.org/10.1016/j.reprotox.2021.08.003.

Morgani, S., Nichols, J., and Hadjantonakis, A.K. (2017). The many faces of Pluripotency: in vitro adaptations of a continuum of in vivo states. BMC Dev. Biol. *17*, 7. https://doi.org/10.1186/s12861-017-0150-4.

Muncie, J.M., Ayad, N.M.E., Lakins, J.N., Xue, X., Fu, J., and Weaver, V.M. (2020). Mechanical tension promotes formation of gastrulation-like nodes and patterns mesoderm specification in human embryonic stem cells. Dev. Cell *55*, 679–694.e11. https://doi.org/10.1016/j.devcel.2020.10.015.

Murphy, V.E., Fittock, R.J., Zarzycki, P.K., Delahunty, M.M., Smith, R., and Clifton, V.L. (2007). Metabolism of synthetic steroids by the human placenta. Placenta *28*, 39–46. https://doi.org/10.1016/j.placenta.2005.12.010.

Parchem, R.J., Ye, J., Judson, R.L., LaRussa, M.F., Krishnakumar, R., Blelloch, A., Oldham, M.C., and Blelloch, R. (2014). Two miRNA clusters reveal alternative paths in late-stage reprogramming. Cell Stem Cell *14*, 617–631. https://doi.org/10.1016/j.stem.2014.01.021.

Patriarca, E.J., Cermola, F., D'Aniello, C., Fico, A., Guardiola, O., De Cesare, D., and Minchiotti, G. (2021). The multifaceted roles of proline in cell behavior. Front. Cell Dev. Biol. *9*, 728576. https://doi.org/10.3389/fcell.2021.728576.

Pera, M.F., and Rossant, J. (2021). The exploration of pluripotency space: charting cell state transitions in peri-implantation development. Cell Stem Cell *28*, 1896–1906. https://doi.org/10.1016/j.stem.2021.10.001.

Pieters, T., and van Roy, F. (2014). Role of cell-cell adhesion complexes in embryonic stem cell biology. J. Cell Sci. *127*, 2603–2613. https://doi.org/10.1242/jcs.146720.

Ramakrishnan, S., Nicolau, D.V., Jr., Langford, B., Mahdi, M., Jeffers, H., Mwasuku, C., Krassowska, K., Fox, R., Binnian, I., Glover, V., et al. (2021). Inhaled budesonide in the treatment of early COVID-19 (STOIC): a phase 2, open-label, randomised controlled trial. Lancet Respir. Med. *9*, 763–772. https://doi.org/10.1016/S2213-2600(21)00160-0.

Rattier, D., Legier, T., Vannier, T., Maina, F., and Dono, R. (2021). Disruption of epithelial integrity drives mesendoderm differentiation in human induced pluripotent stem cells by enabling BMP and ACTIVIN sensing. Preprint at bioRxiv. https://doi.org/10.1101/2021.10.22.465459.

Redmer, T., Diecke, S., Grigoryan, T., Quiroga-Negreira, A., Birchmeier, W., and Besser, D. (2011). E-cadherin is crucial for embryonic stem cell pluripotency and can replace OCT4 during somatic cell reprogramming. EMBO Rep. *12*, 720–726. https://doi.org/10.1038/embor.2011.88.

Riethmacher, D., Brinkmann, V., and Birchmeier, C. (1995). A targeted mutation in the mouse E-cadherin gene results in defective preimplantation development. Proc. Natl. Acad. Sci. USA *92*, 855–859. https://doi.org/10.1073/pnas.92.3.855.

Smith, A. (2017). Formative pluripotency: the executive phase in a developmental continuum. Development *144*, 365–373. https://doi.org/10.1242/dev.142679.

Turner, D.A., Girgin, M., Alonso-Crisostomo, L., Trivedi, V., Baillie-Johnson, P., Glodowski, C.R., Hayward, P.C., Collignon, J., Gustavsen, C., Serup, P., et al. (2017). Anteroposterior polarity and elongation in the absence of extra-embryonic tissues and of spatially localised signalling in gastruloids: mammalian embryonic organoids. Development *144*, 3894–3906. https://doi.org/10.1242/dev.150391.

Turner, D.A., Glodowski, C.R., Alonso-Crisostomo, L., Baillie-Johnson, P., Hayward, P.C., Collignon, J., Gustavsen, C., Serup, P., Schröter, C., and Martinez Arias, A. (2016). Interactions between nodal and Wnt signalling drive robust symmetry-breaking and axial organisation in gastruloids (embryonic organoids). Preprint at bioRxiv. https://doi.org/10.1101/051722.

van den Brink, S.C., Alemany, A., van Batenburg, V., Moris, N., Blotenburg, M., Vivié, J., Baillie-Johnson, P., Nichols, J., Sonnen, K.F., Martinez Arias, A., and van Oudenaarden, A. (2020). Single-cell and spatial transcriptomics reveal somitogenesis in gastruloids. Nature *582*, 405–409. https://doi.org/10.1038/s41586-020-2024-3.

van den Brink, S.C., Baillie-Johnson, P., Balayo, T., Hadjantonakis, A.K., Nowotschin, S., Turner, D.A., and Martinez Arias, A. (2014). Symmetry breaking, germ layer specification and axial organisation in aggregates of mouse embryonic stem cells. Development *141*, 4231–4242. https://doi.org/10.1242/dev.113001.

Vejen Hansen, A., Ali, Z., Malchau, S.S., Blafoss, J., Pinborg, A., and Ulrik, C.S. (2019). Fertility treatment among women with asthma: a case-control study of 3689 women with live births. Eur. Respir. J. *53*, 1800597. https://doi.org/10.1183/13993003.00597-2018.

Washington, J.M., Rathjen, J., Felquer, F., Lonic, A., Bettess, M.D., Hamra, N., Semendric, L., Tan, B.S.N., Lake, J.A., Keough, R.A., et al. (2010). L-Proline induces differentiation of ES cells: a novel role for an amino acid in the regulation of pluripotent cells in culture. Am. J. Physiol. Cell Physiol. *298*, C982–C992. https://doi.org/10.1152/ajpcell.00498.2009.

Yu, L.M., Bafadhel, M., Dorward, J., Hayward, G., Saville, B.R., Gbinigie, O., Van Hecke, O., Ogburn, E., Evans, P.H., Thomas, N.P.B., et al. (2021). Inhaled budesonide for COVID-19 in people at high risk of complications in the community in the UK (PRINCIPLE): a randomised, controlled, open-label, adaptive platform trial. Lancet *398*, 843–855. https://doi.org/10.1016/S0140-6736(21)01744-X.

**Stem Cell Reports, Volume *17***

## Supplemental Information

# Stabilization of cell-cell adhesions prevents symmetry breaking and locks in pluripotency in 3D gastruloids

**Federica Cermola, Filomena Amoroso, Federica Saracino, Eduardo Ibello, Dario De Cesare, Annalisa Fico, Gilda Cobellis, Enrica Scalera, Costanza Casiraghi, Cristina D'Aniello, Eduardo Jorge Patriarca, and Gabriella Minchiotti**

**SUPPLEMENTAL INFORMATION**

Figures S1-S6

Tables S3-S4

Experimental Procedures

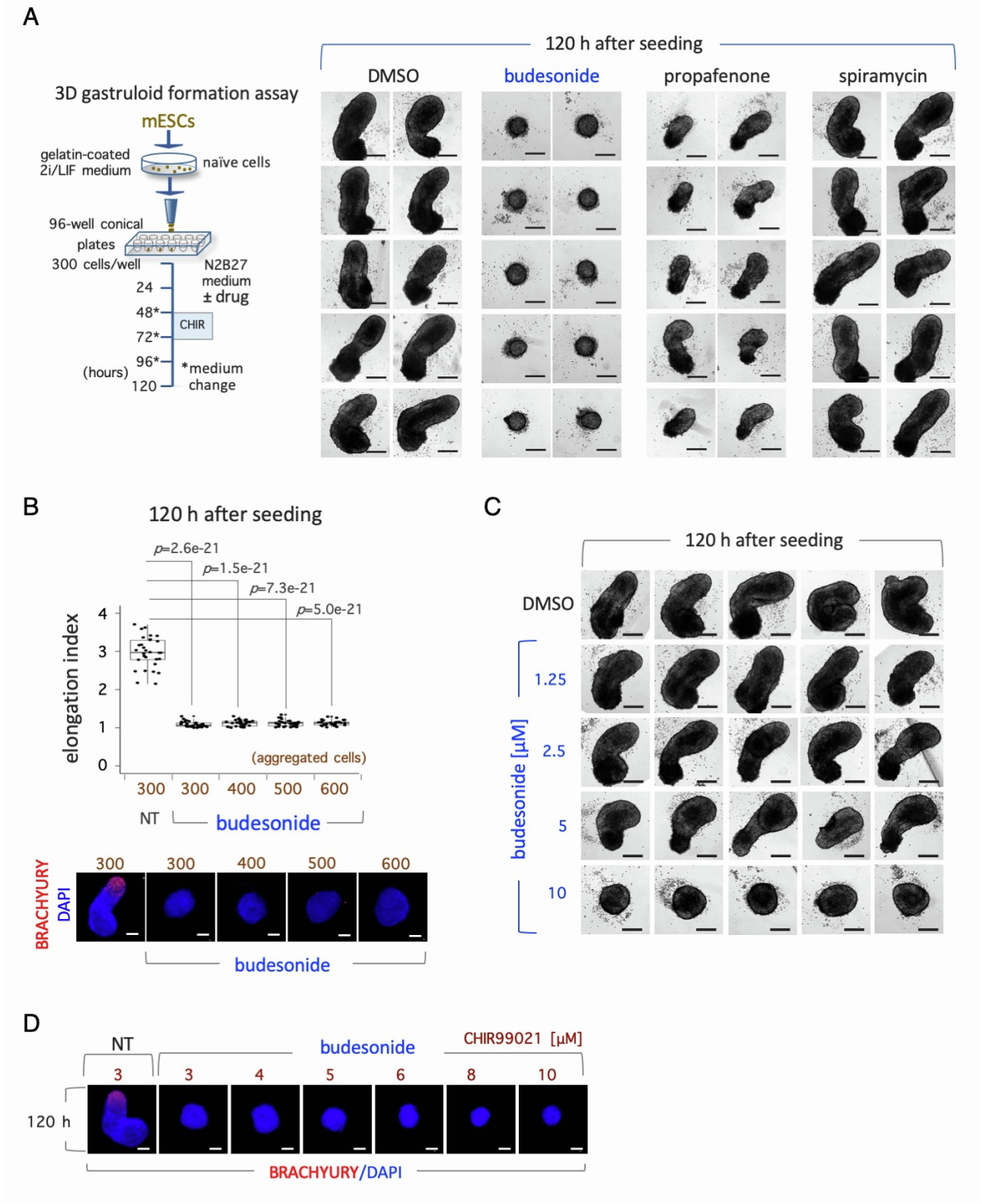


SUPPLEMENTARY FIGURE 1

**Figure S1. Effect of esMT inhibitors, aggregate cell number, and CHIR99021 concentration on gastruloid development.**

(A) Schematic representation of the experimental design. 2i/LIF ESCs were plated on 96-well ultra-low attachment conical plates in N2B27 medium. Representative bright-field images of naïve ESCs -derived gastruloids (120 h) treated with DMSO (control) or the indicated drugs (budesonide, propafenone and spiramycin). The drugs were used at 10 μM and maintained throughout the experiment (bar, 100 μm).

(B) Effect of increased number of aggregated cells (300→600) on budesonide-dependent inhibition of gastruloid formation. Boxplot diagram of the elongation index of control (NT, not-treated with budesonide) and budesonide-treated gastruloids (120 h) (*top*). Representative confocal images of BRACHYURY (*red*) expression in gastruloids ± budesonide (120 h) (*bottom*). Nuclei were counterstained with DAPI (*blue*) (bar, 100 μm).

(C) Dose-dependent effect of budesonide on gastruloid elongation. Representative bright-field images of control (DMSO) and budesonide (1.25→10 μM) -treated gastruloids (bar, 50 μm).

(D) Dose-dependent effect of CHIR99021 on development of budesonide-treated gastruloids. Representative confocal images of BRACHYURY (*red*) expression in 120 h gastruloids ± budesonide (10 μM) ± CHIR99021 (3→10 μM). Nuclei were counterstained with DAPI (*blue*) (bar, 100 μm).

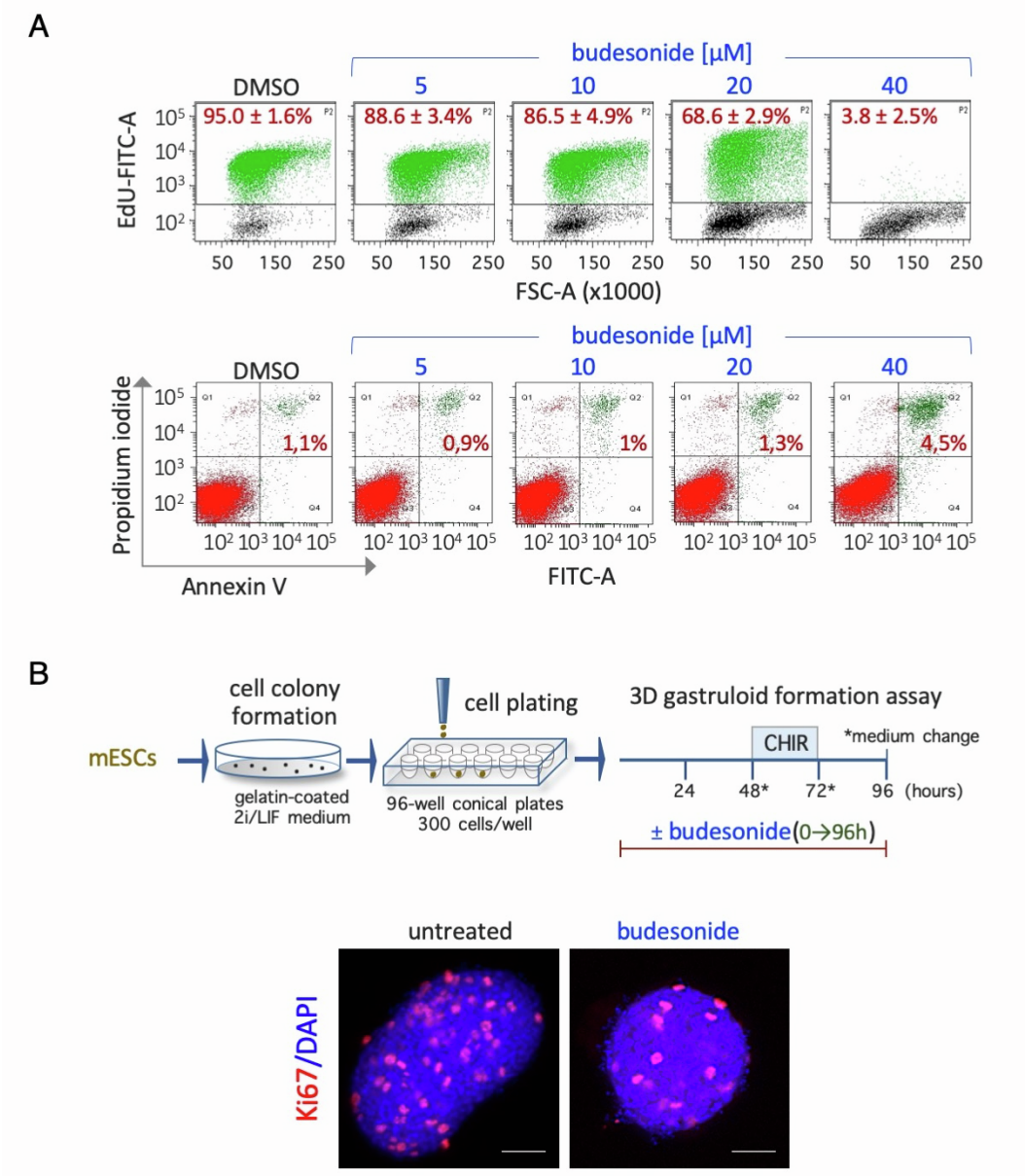


SUPPLEMENTARY FIGURE 2

**Figure S2. Dose-dependent effect of budesonide on ESC proliferation and apoptosis**.

(A) Representative FACS plot showing $EdU^+$ (*top*) and Annexin V/$Propidium^+$ ($AV^+/PI^+$, *bottom*) cells in FBS/LIF ESCs ± budesonide (5→40 μM) at 48 h (data are expressed as mean ± SD; n = 3).
(B) Schematic representation of the experimental design (*top*). Representative confocal images of Ki67 (*red*) expression in gastruloids ± budesonide (10 μM; bottom). Nuclei were counterstained with DAPI (*blue*) (bar, 50 μm).

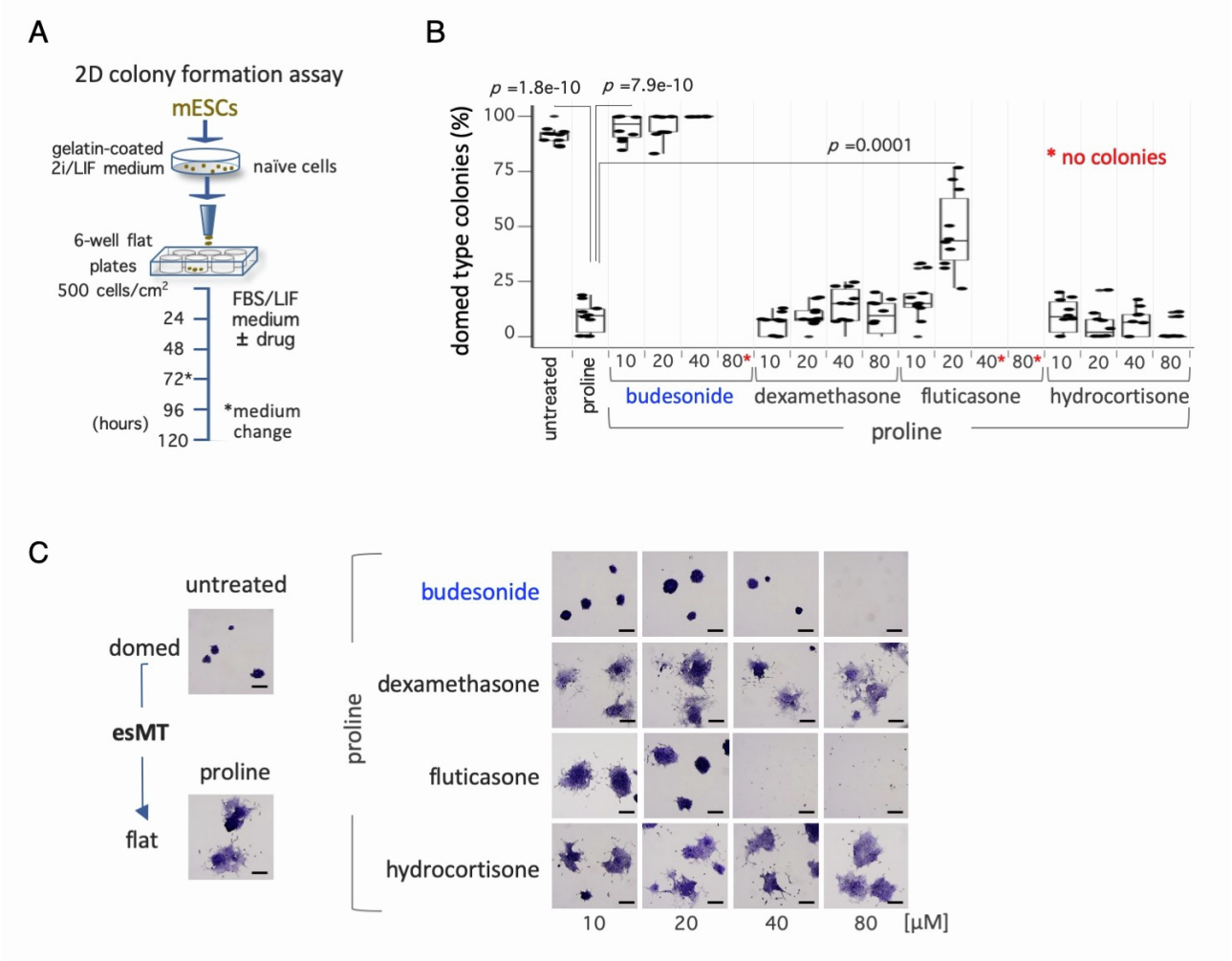


SUPPLEMENTARY FIGURE 3

**Figure S3. Dose-dependent effects of glucocorticoids on esMT.**

(A) Schematic representation of the experimental design. Naïve ESCs were plated (500 cell/cm$^2$) in FBS/LIF medium plus proline (500 μM) ± drugs at the indicated concentrations.

(B) Boxplot diagram showing the fraction (%) of domed-shaped colonies generated in FBS/LIF ± proline ± budesonide, dexamethasone, fluticasone or hydrocortisone at the indicated concentrations (10→80 μM). Red asterisks indicate absence of colonies (n = 2; 10 fields/condition).

(C) Representative bright-field images of crystal violet-stained cell colonies in the different culture conditions (bar, 200 μm).

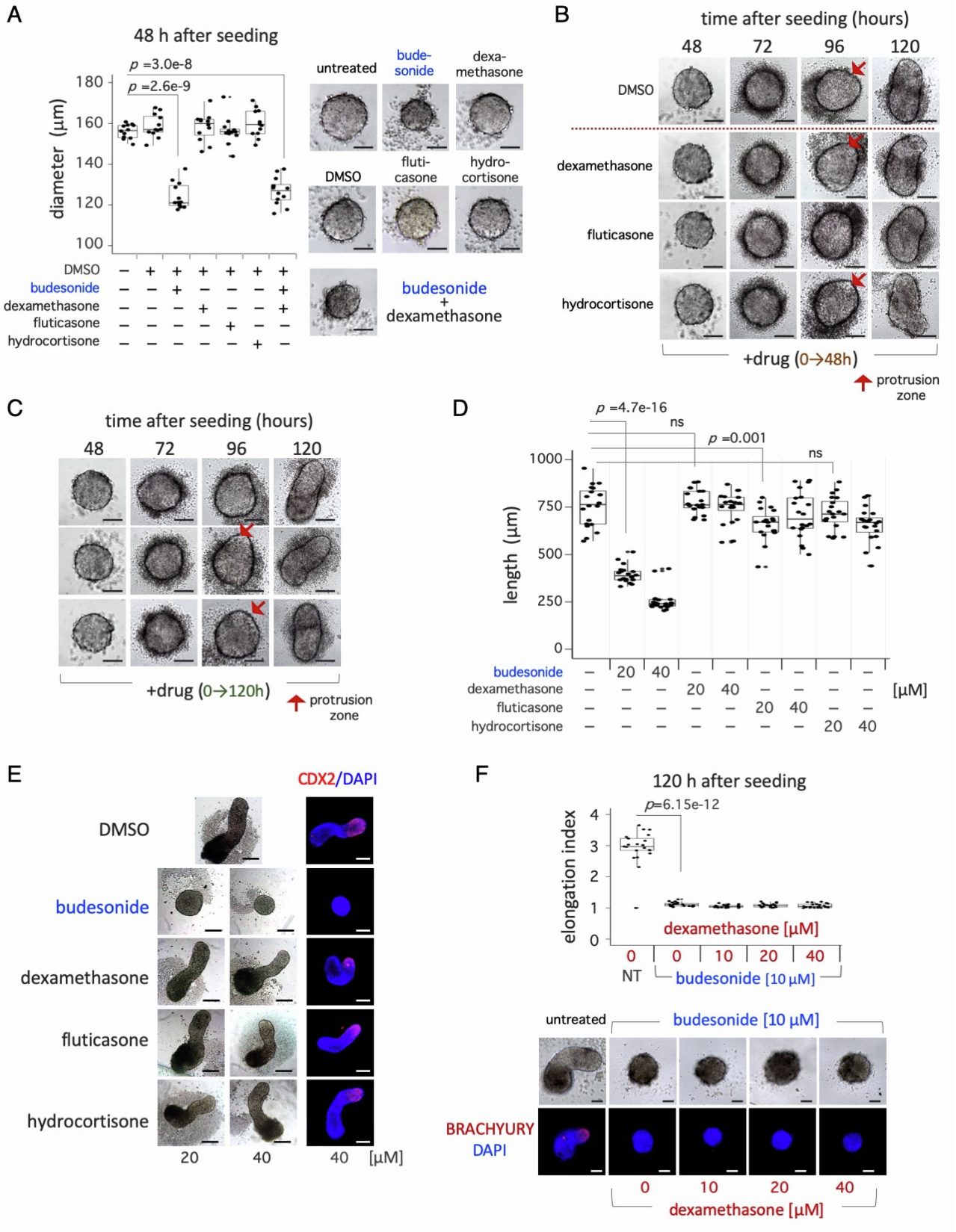


SUPPLEMENTARY FIGURE 4

**Figure S4. Effect of typical glucocorticoids on gastruloid development.**

(A) Boxplot diagram of the diameter distribution (*left)* and representative bright-field images (*right*) of the cell aggregates at 48 h, treated with either the indicated drugs, with DMSO or untreated (bar, 100 μm). The drugs were used either alone or in combination and at a final concentration of 10 μM each (n = 3; 12 aggregates/condition; bar, 100 μm).

(B) Time course representative bright-field images of gastruloids transiently (0→48 h) treated with dexamethasone, fluticasone or hydrocortisone (10 μM). DMSO was used as a control. Arrows indicate apical protrusion zone (bar, 100 μm).

(C) Time course representative bright-field images of gastruloids treated with dexamethasone, fluticasone or hydrocortisone (10 μM) from 0→120 h. DMSO was used as control. Arrows indicate apical protrusion zone (bar, 100 μm).

(D) Dose-dependent effect of glucocorticoids on gastruloid development. Boxplot diagram showing the length of aggregates/gastruloids (120 h) following the indicated treatments (n = 3; 20 gastruloids/condition).

(E) Representative bright-field images of budesonide, dexamethasone, fluticasone or hydrocortisone-treated gastruloids (120 h). The drugs were used at 20 and 40 μM (bar, 100 μm) (*left* and *middle panels*). Representative confocal images of CDX2 (*red*) expression in budesonide, dexamethasone, fluticasone or hydrocortisone (40 μM)-treated gastruloids (120 h) (*right panels*). Nuclei were counterstained with DAPI (*blue*) (bar, 100 μm).

(F) Boxplot diagram of the elongation index of gastruloids ± budesonide (10 μM) and increasing concentration of dexamethasone (10→40 μM) (*top*) (n = 3; 20 gastruloids/condition). Representative bright-field images and confocal images (*bottom*) of gastruloids (120 h) treated with budesonide (10 μM) ± increasing concentration of dexamethasone (10→40 μM) (bar, 50 μm). BRACHYURY expression (*red*) is shown. Nuclei were counterstained with DAPI (*blue*) (bar, 50 μm).

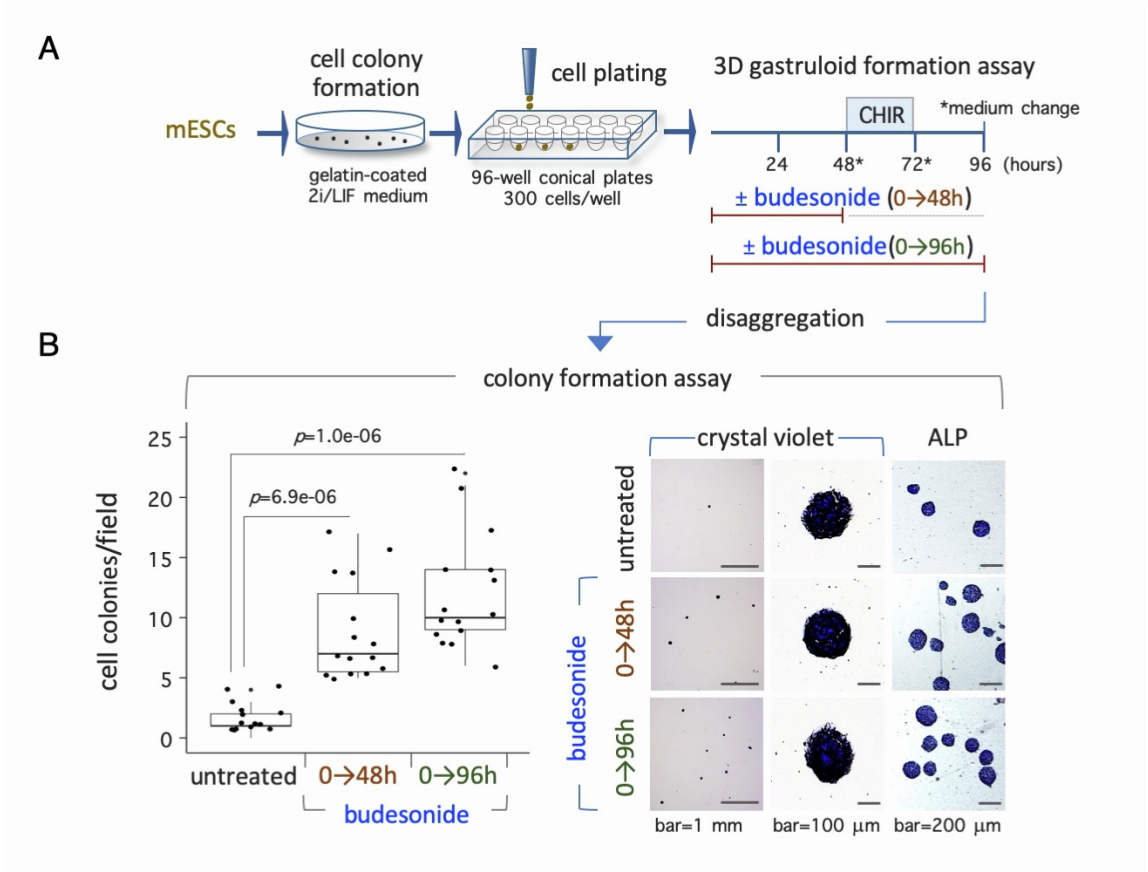


SUPPLEMENTARY FIGURE 5

**Figure S5. Effect of budesonide on ESC self-renewal.**

(A) Schematic representation of the experimental design. Control and budesonide-treated gastruloids were dissociated by trypsin digestion and the cells plated in FBS/2i/LIF medium at either 150 cells/cm$^2$ or 500 cells/cm$^2$ for colonies quantification and alkaline phosphatase assay, respectively, after 120 h in culture.

(B) Boxplot diagram (*left*) showing the number of domed-shaped colonies derived from control (untreated) and budesonide-treated dissociated gastruloids (n = 3; 15 fields/condition). Representative bright-field images of crystal violet and alkaline phosphatase (ALP)-stained colonies derived from control (untreated) and budesonide-treated dissociated gastruloids.

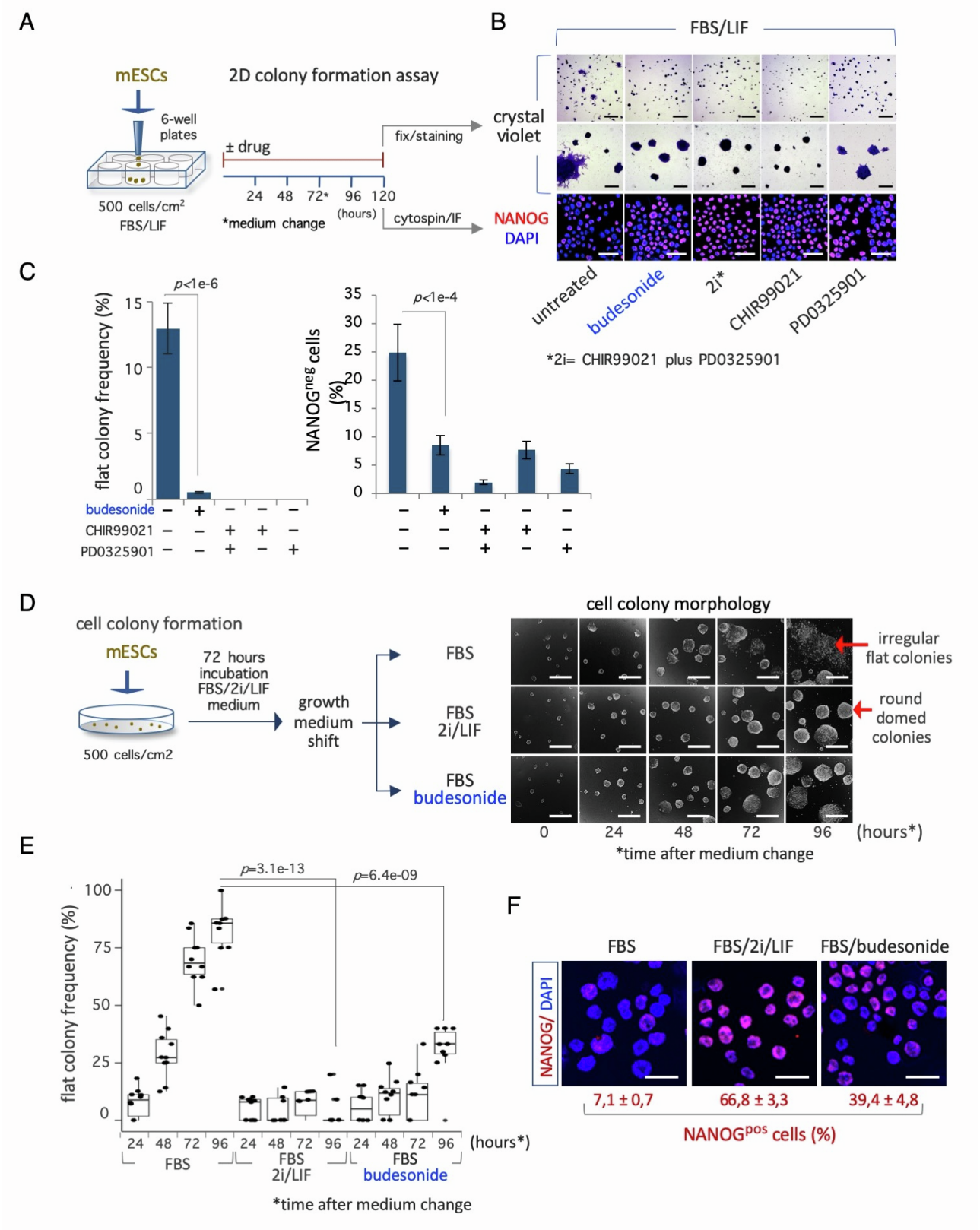


SUPPLEMENTARY FIGURE 6

**Figure S6. Effect of budesonide on exit from naïve pluripotency.**

(A) Schematic representation of the experimental design (*left*); ESCs were plated (500 cells/cm$^2$) and incubated in FBS/LIF medium ± budesonide, 2i, CHIR99021 or PD0325901. After 120 h in culture, cell colonies were either fixed and stained with crystal-violet or harvested and cytospinned.

(B) Representative bright-field images of crystal violet-stained cell colonies (*top*; bar, 200 μm) and representative confocal images (*bottom*) of NANOG expression on cytospin preparation in the different culture conditions. Nuclei were counterstained with DAPI (*blue*) (bar, 100 μm).

(C) Histogram showing the fraction (%) of flat-shaped cell colonies (*left*) and quantification of NANOG$^{neg}$ cells in the different culture conditions (*right*). Data are mean ± SD (n = 3; 10 fields/condition)

(D) Schematic representation of the experimental design (*left*); ESCs were cultured in FBS/2i/LIF medium for 72 h and then shifted to either FBS alone, FBS + budesonide or maintained in FBS/2i/LIF as a control, and imaged every 24 h. Time course representative bright field images of the cell colonies in the different culture conditions (*right*; bar, 200 μm).

(E) Boxplot diagram showing the fraction (%) of irregular flat cell colonies generated from ESCs cultured in either FBS alone, FBS/2i/LIF or FBS + budesonide at the different time points (n=3; 10 fields/condition).

(F) Representative confocal images of NANOG (*red*) expression and quantification of NANOG$^{pos}$ cells in cytospin preparation of ESCs cultured in the indicated conditions (n = 3; 30 fields/condition). Nuclei were counterstained with DAPI (*blue*) (bar, 50 μm).

**Table S3. List of Primary and Secondary Antibodies used in this study, related to Figures 1, 2, 3, 6 and 7**

| Antibody | Source | Cat no. | Application |
|---|---|---|---|
| NANOG | Cell Signaling | 8822 | IF (1:400) |
| OCT4 | Santa-Cruz | sc-8628 | IF (1:100) |
| SOX2 | Cell Signaling | D1C7J | IF (1:100) |
| CDX2 | Cell Signaling | 3977 | IF (1:100) |
| E-CADHERIN | Takara | M108 | IF (1:250) |
| BRACHYURY | Cell Signaling | D2Z3J | IF (1:500) |
| Alexa Fluor 594 Donkey anti-Rabbit IgG | Invitrogen | A21207 | IF (1:400) |
| Alexa Fluor 594 Donkey anti-Goat IgG | Invitrogen | A11058 | IF (1:400) |
| Alexa Fluor 647 Donkey anti-Rabbit IgG | Invitrogen | A31573 | IF (1:400) |
| Alexa Fluor 488 Donkey anti-Rat IgG | Invitrogen | A21208 | IF (1:400) |
| GR(M-20) | Santa-Cruz | sc-1004 | WB (1:500) |
| GAPDH | Abcam | Ab8245 | WB (1:40000) |
| Goat anti-Rabbit | DAKO | P0448 | WB (1:2000) |
| Goat anti-Mouse | DAKO | P0447 | WB (1:10000) |

**Table S4: List of Primers used in this study, Related to Figure 4**

| Gene symbol | Forward (5’-3’) | Reverse (5’-3’) |
|---|---|---|
| *Nr3c1* | ACTCTACCCTGCATGTATGACC | ACTCTTGGCTCTTCAGACCTTC |

## EXPERIMENTAL PROCEDURE

### Gastruloid formation assay (GFA)

At 48 hours after aggregation, CHIR99021 was added to the culture medium at the concentration of 3 μM, or at the indicated concentrations, and maintained for 24 hours. From 72 hours onwards, the medium was refreshed daily up to 120 hours. Gastruloids were imaged using Levenhuk M300 Base Digital Camera for microscopes imaging systems, and the Confocal images were obtained on a Nikon A1 microscope.

To generate gastruloids from FBS/LIF ESCs + proline ± budesonide, ESCs were plated at low density on gelatin-coated plates in FBS/LIF medium supplemented with proline (500 μM) ± budesonide (10μM). After 120 h in culture, cells were dissociated with accutase and gastruloids formation assay was performed.

### Western Blot

Total proteins were extracted in 100 mmol/L Tris pH 8, 140 mmol/L NaCl, 20 mmol/L EDTA, 0,2% SDS, 1% Nonidet P-40 lysis buffer, resolved on SDS-PAGE gels and transferred onto PVDF membranes (iBlot dry Transfer System; Life Technologies). Primary Antibodies were incubated ON at 4°C followed by HRP-conjugated secondary antibodies. Detection was performed with ECL reagents (Pierce, Thermo Scientific). ImageJ software was used for the densitometric analysis.